STUDIES OF THE SOLAR AND TERRESTRIAL RADIATION FLUXES
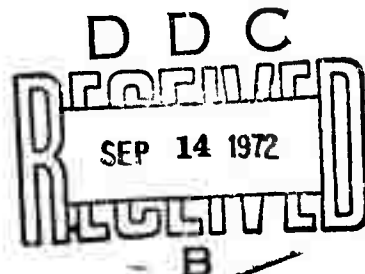## OVER ARCTIC PACK ICE

Sponsored by
Advanced Research Projects Agency
ARPA Order No. 1783

Approved for public release:
distribution unlimited

D D C
RECEIVED
SEP 14 1972
B

The views and conclusions contained in this document are those of the authors
and should not be interpreted as necessarily representing the official policies,
either expressed or implied, of the Advanced Research Projects Agency or the
U. S. Government.

DOCUMENT CONTROL DATA - R & D

(Security classification of title, body of abstract and indexing annotation must be entered when the overall report is classified)

1. ORIGINATING ACTIVITY (Corporate author)	2a. REPORT SECURITY CLASSIFICATION
Geophysical Institute, University of Alaska Gunter Weller	Unclassified
	2b. GROUP

3. REPORT TITLE

Studies of the Solar and Terrestrial Radiation Fluxes Over Arctic Pack Ice

4. DESCRIPTIVE NOTES *(Type of report and inclusive dates)*

Annual Report (Technical Report No. 2) June 1, 1971 - May 31, 1972

5. AUTHOR(S) *(First name, middle initial, last name)*

Gunter Weller, Sue Ann Bowling, K.O.L.F. Jayaweera, Takeshi Ohtake
Stan Parker, Glenn Shaw, Gerd Wendler

6. REPORT DATE	7a. TOTAL NO. OF PAGES	7b. NO. OF REFS
August 1972	74	31

8a. CONTRACT OR GRANT NO.	9a. ORIGINATOR'S REPORT NUMBER(S)
N00014-71-A-0364-0001 b. PROJECT NO. ARPA Order No. 1783	Annual Report Technical Report No. 2
c.	9b. OTHER REPORT NO(S) (Any other numbers that may be assigned this report)
d.	

10. DISTRIBUTION STATEMENT

Unlimited

11. SUPPLEMENTARY NOTES	12. SPONSORING MILITARY ACTIVITY
	Advanced Research Projects Agency

13. ABSTRACT

Our studies have to date concentrated on determining the physical characteristics of pack ice and clouds as they affect the arctic radiation regime. At Barrow, flights through stratus clouds with aircraft-mounted continuous cloud particle samples have determined number and mass density particle size distribution and ice crystal contents. Simultaneously, light intensity and reflectivity measurements have been carried out to determine the optical properties of these clouds. Aircraft-mounted photometers have provided measurements that will allow deductions of aerosol profits up to 13,000 feet; on two occasions these were extended up to 35,000 feet aboard flights by the NASA CV-990 aircraft to the AIDJEX camp in the Beaufort Sea. In addition to measurements of ice nuclei concentrations at Barrow, actinometric observations through frequently thick ice crystal clouds advected from open leads were made on numerous occasions on the AIDJEX camp. Routine monitoring of components of the radiation balance have been carried out at Barrow, Ice Island T-3 and the AIDJEX camp. Of particular interest were the measurements over refreezing leads, both artificially made and natural ones, showing extraordinary modification of the radiation balance during the freezing process. To synthesize all observations, theoretical and computer modeling is playing an increasingly important part in our work.

14	KEY WORDS	LINK A		LINK B		LINK C	
		ROLE	WT	ROLE	WT	ROLE	WT
	Radiation regime Arctic Basin						

STUDIES OF THE SOLAR AND TERRESTRIAL RADIATION FLUXES OVER ARCTIC PACK ICE

Gunter Weller
Sue Ann Bowling
K.O.L.F. Jayaweera
Takeshi Ohtake
Stan Parker
Glenn Shaw
Gerd Wendler

Geophysical Institute
University of Alaska
Fairbanks, Alaska 99701

This is our first Annual Report (Technical Report No. 2) covering the period June 1, 1971 through 31 May 1972 on Contract No. N00014-71-A-0364-0001.

This technical report has been reviewed and is approved.

TABLE OF CONTENTS

Page

INTRODUCTION

G. Weller

Weather and climate in the arctic and sub-arctic regions are strongly affected by the state of the Arctic Ocean and the atmosphere, and by the effective coupling between them. The polar regions occupy the role of the heat sink, as part of the global heat engine which drives the general circulation - studies of these heat sinks are not only important in understanding weather and climate on a regional scale, but in fact, also on a global scale.

In the Arctic Basin, two important components of the environment strongly influence the effectiveness of the heat sink, which owes its existence to net radiative energy losses - these are the presence of perennial pack ice and low stratus cloud decks during summer. ARPA-sponsored research by the University of Alaska into the radiation-related properties of these two media, and into the general solar-terrestrial radiation matrix in the Arctic, commenced during spring 1971. These studies aim to aid in the understanding of the radiation phenomenon in the Arctic atmosphere and at the terrestrial Arctic surface, and ultimately relate to considerations of the heat budget of the polar regions and to climate modifications and controls in that area. Our studies to date have concentrated on determining the physical characteristics of both pack ice and clouds, as they affect the Arctic radiation regime. At Barrow, flights through stratus clouds with aircraft-mounted continuous cloud particle samplers have determined number and mass densities, particle size distributions and ice crystal contents of these clouds over a wide temperature range. Simultaneously, light intensity and reflectivity measurements have been carried out to determine the optical properties

5

of these clouds. A study of precipitation mechanisms is also underway.

Aircraft-mounted photometers have provided measurements that will allow deduction of aerosol profiles up to 13,000 feet; on two occasions, these were extended up to 35,000 feet aboard flights by the NASA CV-990 aircraft to the Arctic Ice Dynamics Joint Experiment (AIDJEX) camp in the Beaufort Sea. Although the air is fairly "clean" over the Arctic Ocean, ice crystal aerosols are present, and are important in scattering incoming radiation. In addition to measurements of ice nuclei concentration at Barrow, actinometric observations through frequently thick ice crystal clouds advected from open leads were made on numerous occasions on the AIDJEX camp.

Routine monitoring of components of the radiation balance have been carried out at Barrow, Ice Island T-3 and the AIDJEX camp. Coupled with this were studies of surface inhomogeneities, such as hummocks, snow dunes, leads and pressure ridges, and the effects of these features on the surface albedo and temperature. Of particular interest were the measurements over refreezing leads, both artificially-made and natural ones, showing extraordinary modification of the radiation balance during the freezing process. Light extinction measurements in snow, ice and sea water, using photocells, allowed the construction of a typical extinction nomogram for these substances.

To synthesize all observations, theoretical and computer modeling is playing an increasingly important part. We hope to pursue this latter aspect much more vigorously in the future.

The authors of this report are:

Dr. Sue Ann Bowling, Assistant Professor of Geophysics

Dr. K.O.L.F. Jayaweera, Assistant Professor of Geophysics

6

Dr. Takeshi Ohtake, Associate Professor of Geophysics

Mr. Stan Parker, Research Assistant

Dr. Glenn Shaw, Assistant Professor of Geophysics

Dr. Gunter Weller, Associate Professor of Geophysics

Dr. Gerd Wendler, Associate Professor of Geophysics

All are staff members of the Geophysical Institute of the University of Alaska.

The results presented in this report are incomplete. The final report on this contract will be available by spring 1973.

7

I. RADIATION REGIME OF THE ARCTIC BASIN - STUDIES AT T-3, AIDJEX SITES AND BARROW

G. Weller and S. Parker

Routine Monitoring Program

Radiation fluxes of short-wave incoming (global), short-wave reflected and net all-wave radiation were measured continuously through summer 1971 at both Barrow (27 May - 5 September) and T-3 (22 April - 29 October). Eppley precision pyranometers and Fritschen net radiometers were used. Figure 1 shows the installation of the equipment at T-3 in April 1971. A Davos PD-1 hemispherical all-wave sensor can be seen mounted on the tripod in the foreground of the photo. This instrument was used on occasions to obtain the outgoing all-wave radiative flux. This installation was replaced by four Eppley pyranometers (2 short-, 2 long-wave) in May 1972 and has been operating since at T-3. A similar set of sensors was used on the AIDJEX main camp in the Beaufort Sea during April 1972.

Icing problems during 1971 were severe on occasions, more so at T-3 than at Barrow, and frequent cleaning of the instruments and correction of the records was necessary. During 1972, this was made unnecessary by the use of a warm-air blower system, especially designed and built for the purpose, which kept the sensors completely free of frost deposits. Table 1 shows a typical computer printout of data for T-3 and Barrow. Monthly summaries of total daily integrated radiation values will also be listed in the final tabulations. Figure 2 shows a plot of typical values of global and net radiation when skies were clear at both stations. This occurred during the summer solstice on 21 June 1971 when Barrow (latitude 71°N) and T-3 (latitude 85°N) were approximately 2000 km apart. The effect of latitude on the diurnal variations of the radiative components is clearly recognizable.

8
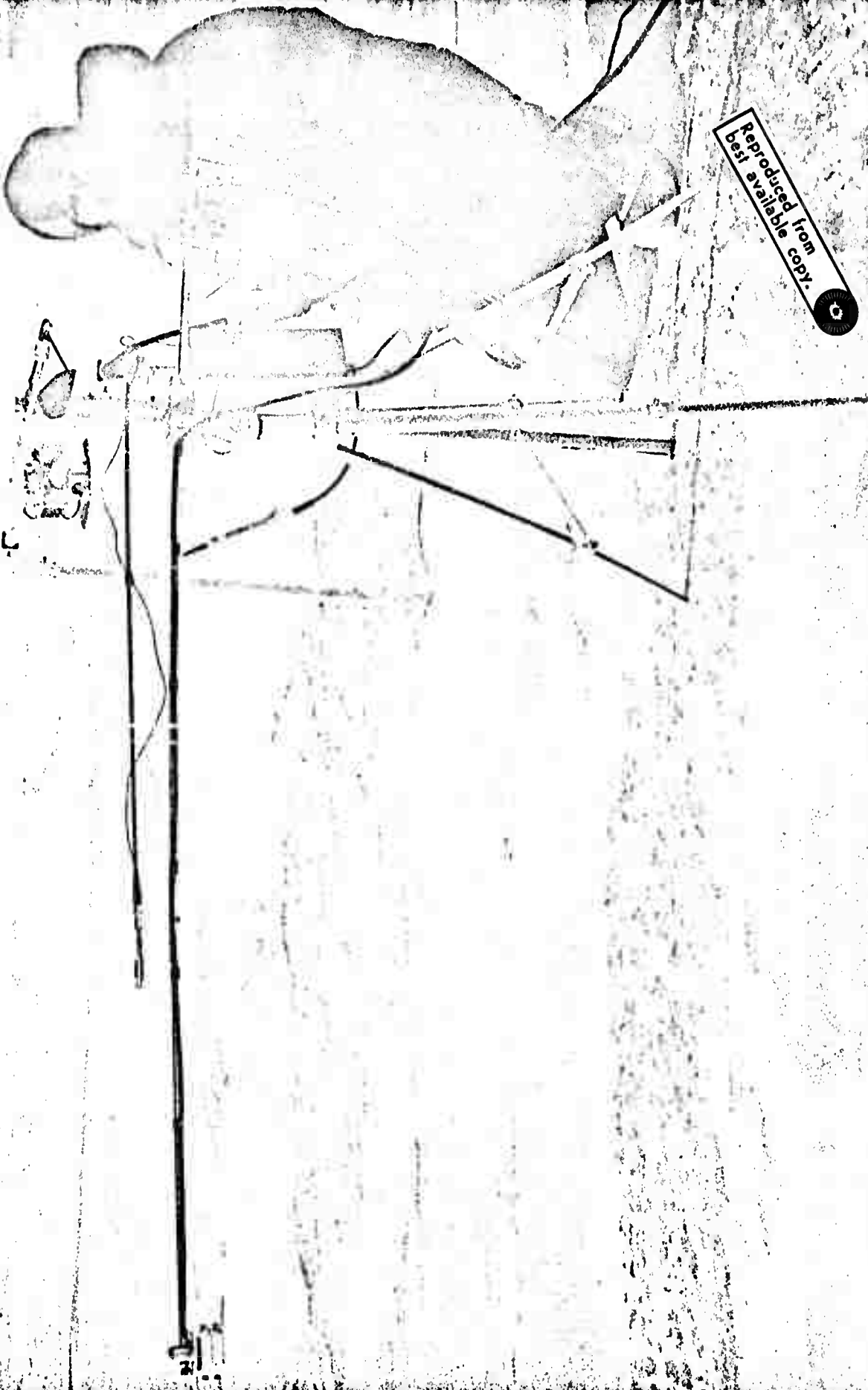
Fig. 1 Installation of radiation equipment at T-3 in April 1971.
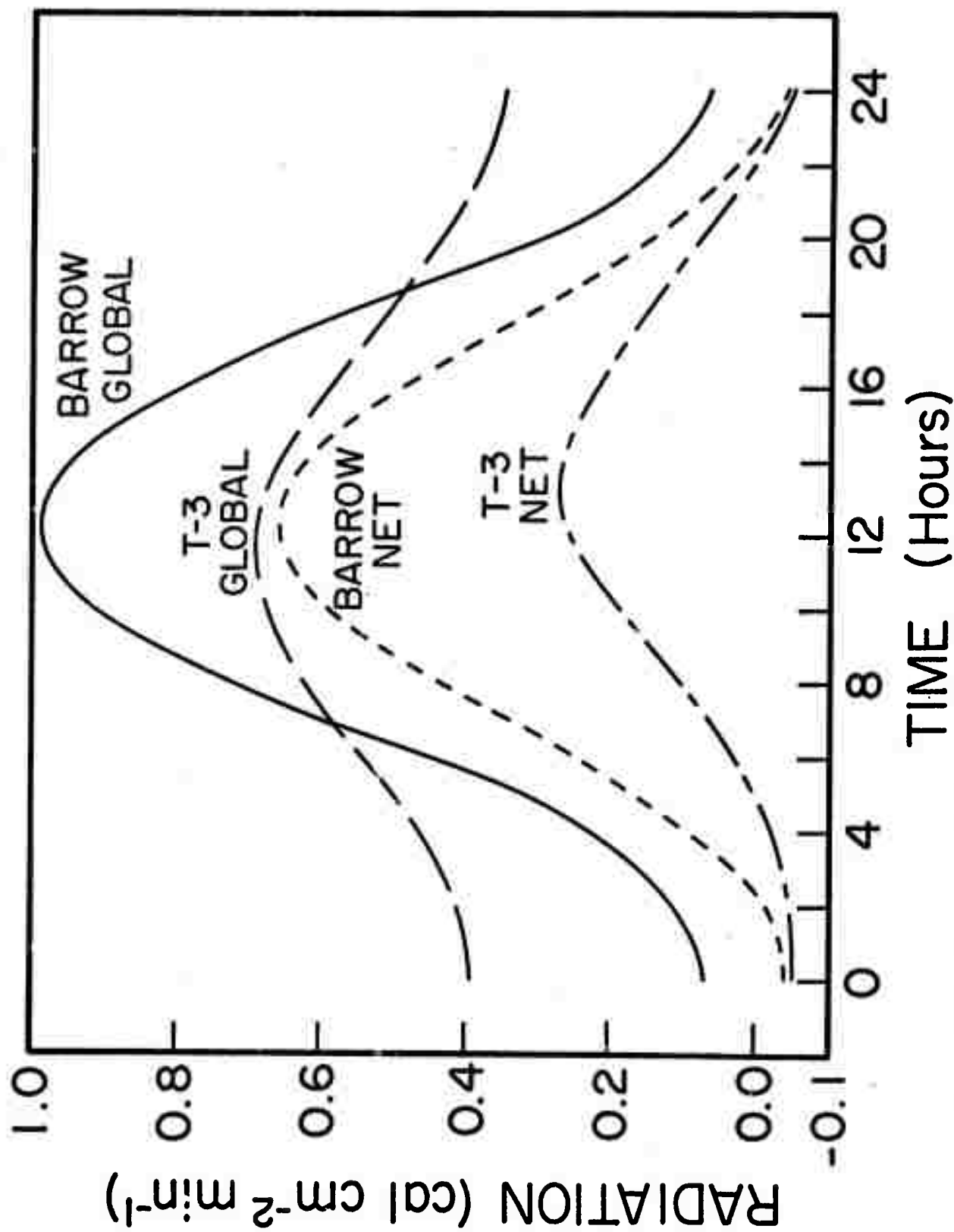
Fig. 2 Global and net radiation at Barrow and T-3 on 21 June 1971, with clear skies at both stations.

10

T-3 RADIATION DATA

CAL/(CM MIN)²

TIME	SHORT IN	SHORT OUT	ALBEDO	SHORT NET	ALL NET	LONG NET
DATE= 5/31/71						
000	0.42	0.40	0.94	0.02	-0.01	-0.03
100	0.46	0.42	0.93	0.03	-0.01	-0.03
200	0.50	0.44	0.88	0.06	0.02	-0.04
300	0.55	0.46	0.85	0.08	0.03	-0.04
400	0.58	0.48	0.84	0.09	0.05	-0.06
500	0.62	0.50	0.80	0.12	0.06	-0.05
600	0.64	0.51	0.80	0.13	0.08	-0.05
700	0.66	0.53	0.80	0.13	0.10	-0.03
800	0.66	0.54	0.81	0.13	0.10	-0.02
900	0.68	0.54	0.80	0.12	0.11	-0.02
1000	0.66	0.54	0.81	0.13	0.10	-0.01
1100	0.64	0.51	0.80	0.13	.09	-0.01
1200	0.60	0.50	0.83	0.10	0.07	-0.03
1300	0.57	0.47	0.84	0.09	0.05	-0.03
1400	0.53	0.45	0.88	0.08	0.04	-0.02
1500	0.49	0.43	0.90	0.05	0.03	-0.02
1600	0.45	0.40	0.92	0.04	-0.01	-0.04
1700	0.42	0.38	0.95	0.03	-0.02	-0.04
1800	0.39	0.37	0.96	0.02	-0.02	-0.04
1900	0.37	0.35	0.97	0.02	-0.04	-0.05
2000	0.36	0.35	0.95	0.01	-0.03	-0.05
2100	0.36	0.34	0.98	0.01	-0.03	-0.04
2200	0.37	0.36	0.98	0.01	-0.03	-0.04
2300	0.39	0.38	0.99	0.01	-0.03	-0.03

CAL/(CM DAY)²

	SUM	SUM	MEAN	SUM	SUM	SUM
	741.6	660.4	0.88	101.2	50.0	-51.2

BARROW RADIATION DATA

CAL/(CM MIN)²

SHORT IN	SHORT OUT	SHORT NET	ALBEDO	ALL NET	LONG NET
0.04	0.04	0.0	0.92	-0.02	-0.02
0.04	0.04	0.0	0.92	-0.01	-0.01
0.03	0.03	0.0	0.95	-0.01	-0.01
0.05	0.05	0.0	0.91	-0.01	-0.0
0.12	0.11	0.01	0.88	0.01	-0.03
0.25	0.21	0.04	0.95	0.01	-0.03
0.30	0.26	0.04	0.86	0.02	-0.02
0.32	0.28	0.04	0.88	0.02	-0.05
0.52	0.45	0.07	0.86	0.03	-0.07
0.67	0.57	0.10	0.86	0.02	-0.07
0.72	0.63	0.09	0.87	0.05	-0.09
0.87	0.75	0.14	0.84	0.05	-0.12
0.74	0.70	0.1	0.81	0.02	-0.11
0.81	0.61	0.13	0.83	0.03	-0.11
0.80	0.67	0.14	0.84	0.03	-0.09
0.80	0.66	0.12	0.82	0.02	-0.12
0.50	0.42	0.14	0.94	0.02	-0.06
0.54	0.46	0.08	0.85	0.03	-0.05
0.33	0.28	0.05	0.86	0.01	-0.04
0.25	0.21	0.04	0.82	0.02	-0.02
0.21	0.17	0.04	0.81	0.02	-0.02
0.13	0.11	0.02	0.82	0.01	-0.01
0.04	0.04	0.0	0.90	-0.01	-0.01

CAL/(CM DAY)²

SUM	SUM	SUM	MEAN	SUM	SUM
595.8	503.4	92.4	0.88	22.7	-70.2

EXPLANATIONS
SHORT IN= SHORT WAVE RADIATION INCOMING
SHORT OUT=SHORT WAVE RADIATION OUTGOING
SHORT NET=NET SHORT WAVE RADIATION
ALBEDO= SHORT OUT/SHORT IN
ALL NET= NET LONG AND SHORT WAVE RADIATION
LONG NET= NET LONG WAVE RADIATION

TABLE 1

SAMPLE LISTING OF RADIATION DATA FOR BARROW AND T-3, 31 MAY 1971.

11

These basic measurements are useful in synthesizing a radiation climatology of the Arctic Basin, particularly if carried out over longer time spans, as proposed by us. With an array of stations, the dynamic nature of the interaction between cloud advection and formation and the radiation balance can also be studied. Such a high-density array will be provided by the full-scale AIDJEX station grid during 1974/75, in which we propose to carry out these radiation studies.

Ice Surface Temperatures

An important objective of the field studies during spring 1972 has been to extend the single-point observations at the stations listed above, to a greater spatial consideration of surface inhomogeneities. These inhomogeneities are present in the form of different types of ice, snow cover, ice-free and refrozen leads of various thickness, melt-ponds, hummocks and ice ridges. Spatial sampling of these types of surfaces have included measurements of albedoes and radiative surface temperatures. A study by Maykut and Untersteiner (1969) has shown how even small differences in albedo can be critical in considerations of the stability of a sea ice cover.

Radiative surface temperatures were measured at the AIDJEX camp in the spring of 1972, when their immediate use as ground-truth for the NASA remote sensing overflights was greatest. The basic instrumentation used for this purpose was a PRT-5 infrared thermometer. Table 2 summarizes the results of these measurements. It is clear that despite the relative homogeneity of multi-year pack ice surfaces in spring, large temperature differences can exist. This means that single-point observations at the surface have to be examined carefully, before being used as ground-truth data for aerial remote-sensing.

12

TABLE 2

Surface Temperature Differences of Multi-Year Pack Ice in Spring

Weather Conditions	Surface Temps of Sloping Ice Surfaces With a Flat Surface (°C)		ΔT max (°C)
	Sunny Side	Shaded Side	
Clear sky, calm	+3.5	−3.8	7.3
Clear sky, light wind	+1.2	−1.8	3.0
Thin clouds, light wind	+0.7	−0.3	1.0
O/cast, strong winds	0	0	0

This tentative table represents the results of 36 series of measurements; complete analysis of additional measurements on a more rigorous basis in in progress.

Radiative Characteristics of Refreezing Leads

Much more dramatic, of course, is the dynamic temperature change of refreezing leads. This was measured at the AIDJEX main camp in April 1972, both on naturally occurring and artificially created leads, and is shown in Figure 3, together with freezing rates and albedoes of the same leads. Mean air temperatures were constant at around −25°C during the studies so that steady-state conditions can be assumed. Also, no snow fell, or was blown on the refreezing leads during the period of observation. Thermal coupling with the water under the ice is very strong, until the ice reaches a thickness of about 20 cm, but even when the ice is a meter thick, the ice surface temperature is still up to 2°C warmer than the near-surface air temperature. A snow cover on the ice, because of its low thermal conductivity, will couple much more strongly with the atmosphere, so that temperature differences between air and lead surface will be substantially reduced.

Albedo measurements over the refreezing leads show rapid increases with ice thickness, except for a short initial decrease. This latter effect occurs when the mirror reflectivity of the open water surface at low solar elevations
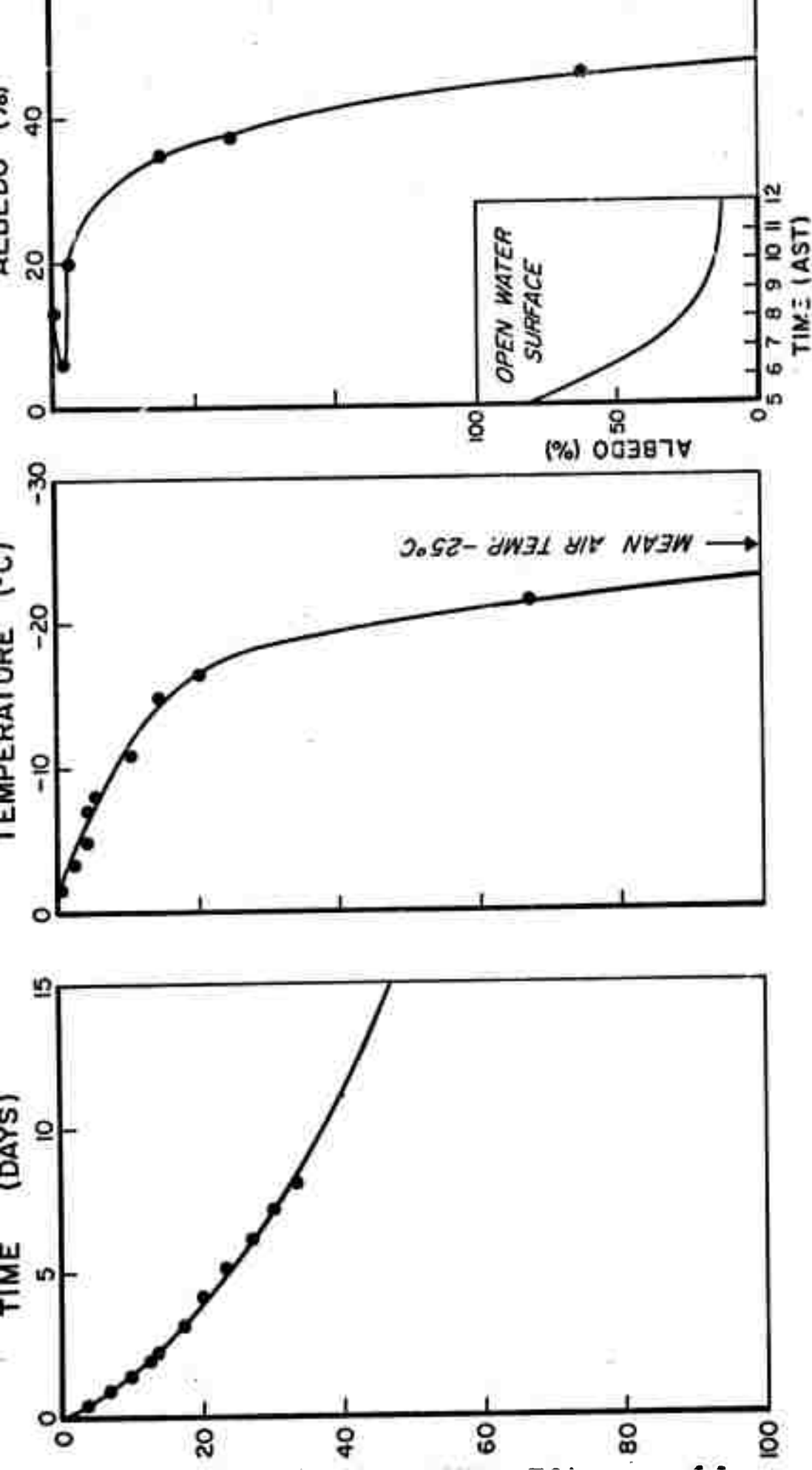
FIG. 3.: RATE OF FREEZING, SURFACE TEMPERATURES AND ALBEDOS OF A REFREEZING LEAD
AIDJEX, APRIL 1972

is reduced due to ice crystal formation on that surface. From these values and from continuous measurements of incoming short-wave and long-wave radiation, radiation balances can now be computed for the lead. These are shown by four days following freeze-up in Figure 4. By comparison with the measured radiation balance of multi-year ice, it is seen that the open lead looses about twenty times more radiative energy to the atmosphere than the thick multi-year ice. These measured values agree well with the estimates by both Badgley (1966) and Doronin (1969) for early April. As freezing of the lead continues, its radiation balance approaches that of the multi-year ice asymptotically. Four days after freeze-up it is still six times higher, the multi-year ice balance having remained constant under clear skies and identical temperature conditions. The importance of leads in the heat balance of the Arctic atmosphere is thus clearly shown. In addition, latent heat fluxes from the relatively warm lead surfaces also contribute heat to the atmosphere. The open leads may well supply two orders of magnitude more thermal energy than multi-year ice, as suggested by Badgley (1961).

Light Extinction in Snow, Ice and Sea Water

Inhomogeneity of the pack-ice surface also strongly affects the transmission of radiation through the ice. This applies in particular to the depth of snow on the ice surface, since snow has a much higher extinction coefficient than ice. To measure the extinction processes in sea ice and sea water, small (2 x 1 cm) selenium photocells, the spectral responses of which cover the solar spectrum, were lowered through small boreholes in the typical wind-packed spring snow of density 0.36 gm cm^{-3}, irregularly covering the pack ice, was determined by placing a large block of snow over a photocell, and reducing its thickness by cutting sections from the top. Exponential extinction occurred in all three media, as expected, and as shown elsewhere

15

FIG. 4: RADIATION BALANCE OF A REFREEZING LEAD
AIDJEX CAMP, APRIL 1972
(CLEAR SKIES, TEMPS: −22°C ≥ T ≥ −30°C, MEAN: −26°C)

* Mean of March and April values
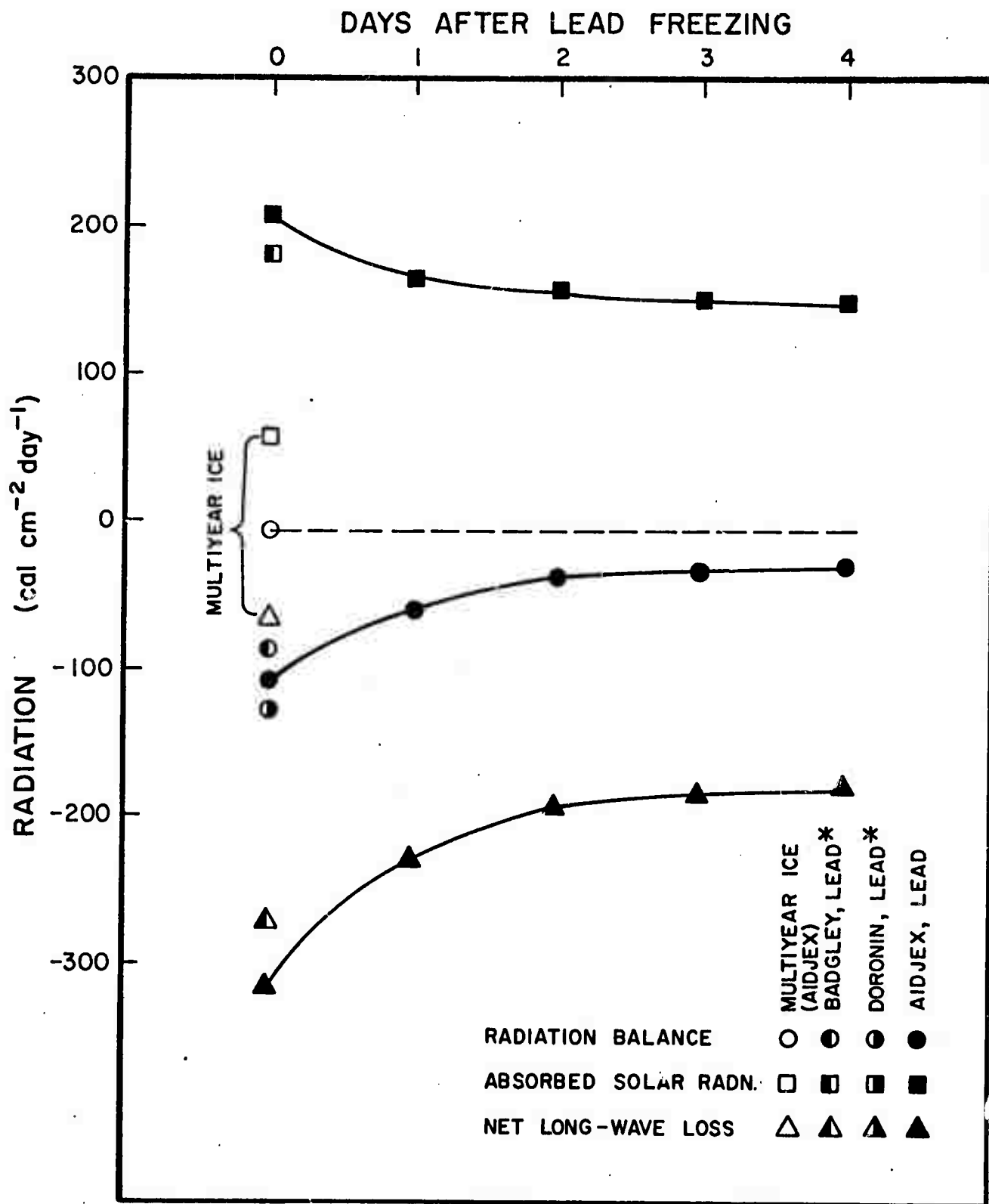
by Weller and Schwerdtfeger (1967) and Weller (1969).

The exponential extinction coefficients for snow, ice and water were
0.29, 0.012 and 0.0025 cm^{-1}, respectively. A nomogram can be constructed
from these results (Figure 5) from which the light intensity at any vertical
level below the surface can be quickly read, for any combination of thick-
nesses of snow, ice and water. For example, the light intensity at the
ice-water interface under 10 cm snow and 2 m ice, is 0.7% of that penetrating
the snow surface; for no snow and 3 m ice it is about 3%.

Cloud Albedoes

The arctic radiation regime is dominated by low stratus cloud decks
during summer, which have a considerable effect on the radiation balance
of the surface and the atmosphere (Fletcher, 1965). Our efforts to define
the role of stratus clouds in the arctic atmosphere so far have concentrated
on determining the physical and optical properties of these clouds, through
a series of measurements with aircraft-mounted sensors. These flights took
place at Barrow with light aircraft during August and September 1971, and
again in April and May 1972, flying through multi-layered cloud decks up
to altitudes of 4000 meters.

Cloud albedo measurements were carried out at the same time as cloud
sampling flights (Section III), using a light-weight CSIRO albedometer,
mounted forward of the wing and attached to the strut of a Cessna 180 air-
craft. Figure 6 shows typical results, indicating the wide spectrum of
values obtained when the cloud cover is thin. Aircraft flying altitudes
were 200 meters above the cloud, so that fifty percent of the sensor re-
sponse comes from a cloud surface area 400 meters in diameter. This is a
small area in terms of resolution elements of meteorological satellites,
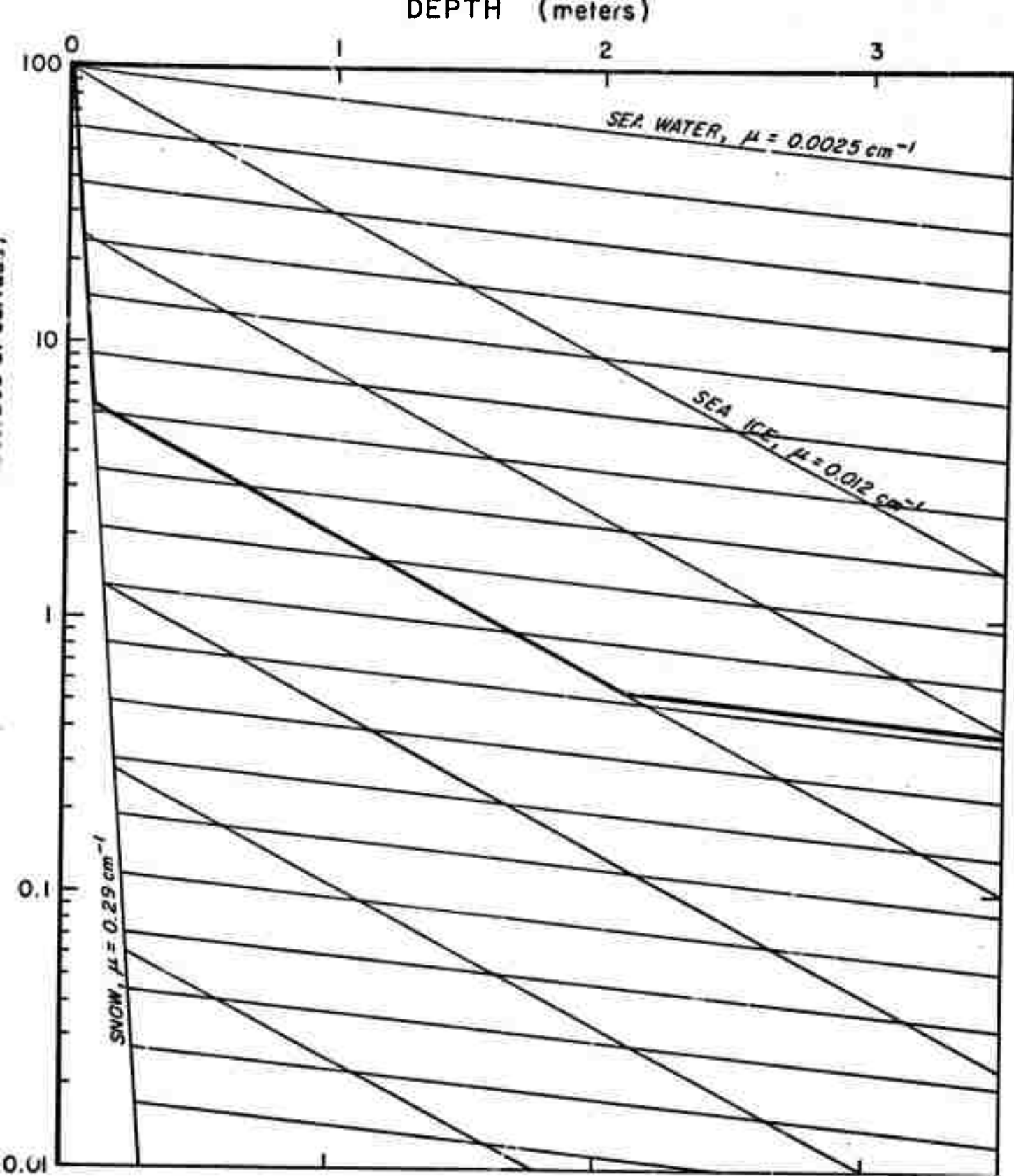so that spatial variations of cloud albedoes due to holes will probably

17

FIG. 5: NOMOGRAM FOR THE DETERMINATION OF LIGHT INTENSITIES IN A THREE-LAYER SYSTEM: SNOW, SEA ICE, SEA WATER AIDJEX, 1972 **18**

The example (heavy line) shows light intensities for 10 cm of snow overlying sea ice 2 meters thick.
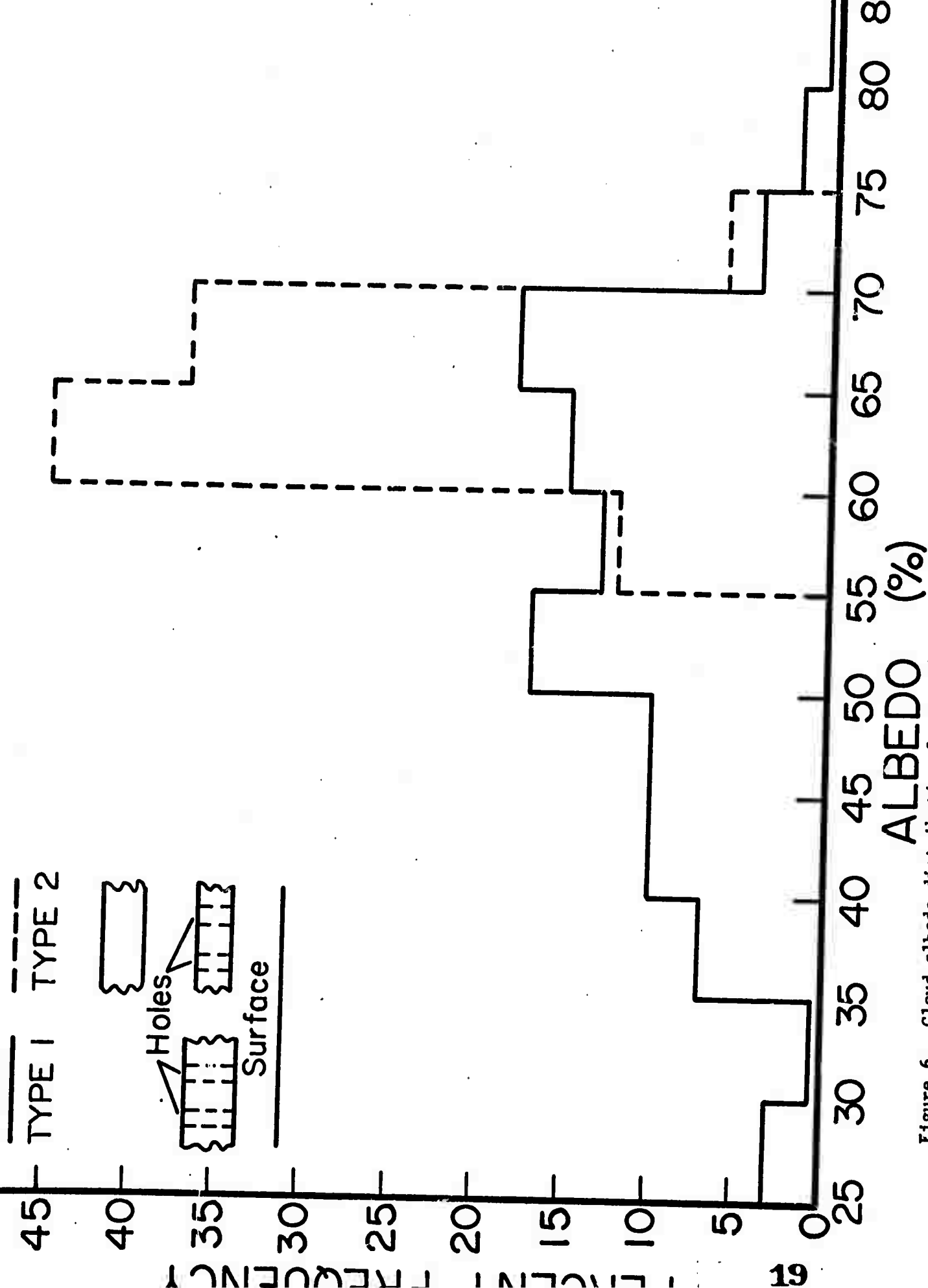
Figure 6. Cloud albedo distribution for single and two-layered cloud deck at Barrow.

19

not be seen, except in the mean values. On the other hand, satellites such as the proposed ERTS-series will have several resolution elements covering the 400 meter diameter area, and will thus see the holes. The measured values appear to be in good agreement with those obtained at lower latitudes and reported by Fritz (1957) despite the fact that the composition of the clouds is somewhat different (Section III). It is clear that both cloud thickness and the presence of holes in the cloud will affect the longwave as well as the shortwave radiative exchange with the upper atmosphere and space. The latter effect is discussed in Section II.

Ice Surface Albedos

In a similar fashion, albedo values for the pack ice surface were determined at the AIDJEX camp in spring 1972. The instrumentation in this case consisted of two Eppley precision pyranometers mounted on top and under the rear fuselage of a Twin Otter aircraft. The flights, primarily photographic missions at regular intervals, consisted of one run of 10 km length at 12,000 feet over the AIDJEX camp, followed by 10 runs at 5,000 feet, covering an area 10 x 10 km over the camp. Finally, a low run at 1,500 feet was made over the camp. As with the cloud albedo measurements, recording was on a portable single-channel high-speed line recorder, recording incoming radiation for 5 minutes, followed by 10 minutes of reflected radiation. Measurements were only made when the sky was completely clear. All data are not analyzed yet, but initial results are shown in Figure 7.

As far as these tentative results allow analysis, the following statements can be made. The mean albedo of 78% for multi-year ice agrees well with single-point surface measurements. The overall frequency distribution is skewed, due to the presence of many refrozen leads, generally less than a meter thick and more than 1 km wide. From the histogram for all observations

20

FLYING
ALTITUDE

12,000 FT

5,000 FT

1,500 FT

NUMBER
OF
OBSERVATIONS

150

100

50

0

Old leads   Multiyear ice
< 1 m thick
> 1 km wide
Old leads ~20% of surface

75 76 77 78 79 80
ALBEDO (%)
6 APRIL

75 76 77 78 79 80
ALBEDO (%)
13 APRIL

75 76 77 78 79 80
ALBEDO (%)
TOTAL

21
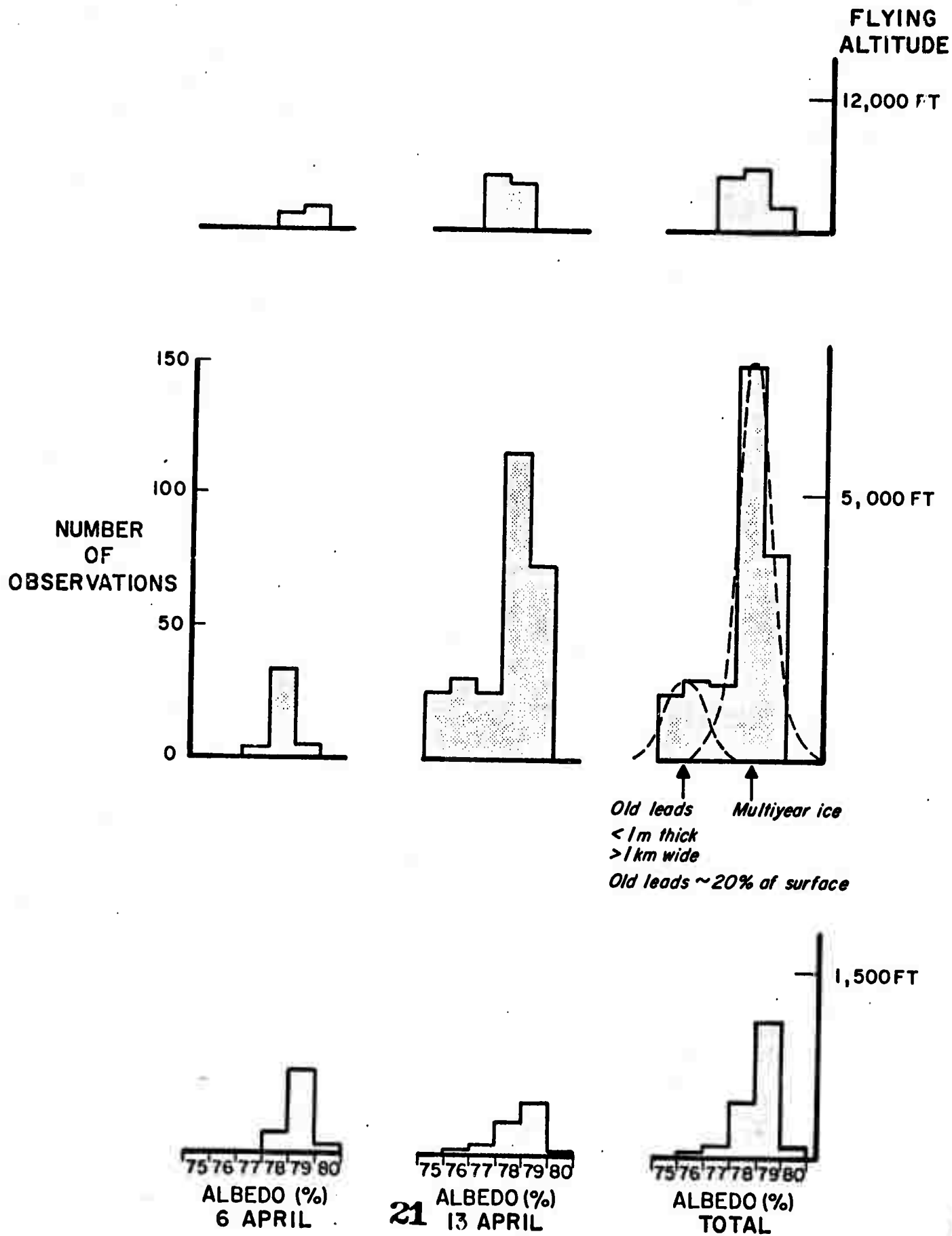
from 5,000 feet height, it appears that they cover approximately 20% of the 10 x 10 km area around the AIDJEX camp. Their albedo is about 75%; this relatively high value is due to snow deposits on the leads. Smaller features with different albedos are not seen in the historgrams - also the paucity of data analyzed so far does not yet allow comparison of data from various flight altitudes.

II. EFFECTS OF ARCTIC STRATUS CLOUDS ON THE RADIATION REGIME

Gerd Wendler

The arctic summer stratus cloud cover is one of the most persistent cloud systems of the world and consequently, it has a great influence on the climate. Its importance has been pointed out by Fletcher (1966) and in the NAS study "Polar Research" (1970). Theoretical as well as experimental investigations of the relation between incoming solar radiation and clouds have been carried out by Albrecht (1933), Hewsen (1943), Neiburger (1948), Haurwitz (1948), Vowinckel and Orvig (1962a,b), Loewe (1963), Franceschini (1968) and many more.

In this study the influence of stratus clouds on the incoming radiation was investigated for Barrow, Alaska. The radiation (incoming and reflected) was measured with Eppley pyranometers, while cloud observations were obtained from the Weather Bureau records for Barrow. So far, the study has been carried out only for the month of June. This month was chosen because (a) the solar height is relatively large, so that the energy received from the sun is substantial and (b) this is the month in which a great change in the surface albedo occurs. The experimental site was located 3 km inland from Barrow so that the influence of the Arctic Ocean, which can have a very different albedo than the tundra, was negligible.

First an investigation of the dependence of the radiation received

22

on ceiling height of stratus clouds was carried out. Figure 1 shows, for three classes of ceiling heights, no systematic difference in the incoming radiation. This is to be expected, as not the height but the thickness of the cloud cover and the density and size distribution of the cloud droplets will determine the reflection, absorption and transmission of the incoming radiation.

In Figure 2, the amount of incoming radiation is shown as a function of thickness. (The cloud thickness was estimated from the humidity data of the radiosonde ascents at Barrow.) One sees that, with increasing cloud thickness and especially for multi-layered clouds, the amount of radiation received on the ground decreases; however, there is quite a substantial amount of scatter in the data.

Multiple reflection between the ground surface and the lower portion of the cloud is of great interest, since it has considerable influence on the amount of energy received at the surface. If one assumes that a cloud scatters the light in all directions equally, which is approximately true for a cloud of sufficient thickness, then the schematic simplified diagram given in Figure 3 is applicable. It can be seen that the energy, which will be received on the surface, $I_{surface}$, is:

$$I_{surface} = I_\alpha (1 - a)(1 - \alpha)(1 + \sum_{n=1}^{\infty} z^n)$$

with $z = (1 - a)\alpha\beta$

I_α = energy received above the cloud per cm^2 horizontal surface

a = absorption in cloud

α = albedo of cloud

β = albedo of cloud

One can see that the multiple reflection becomes increasingly important
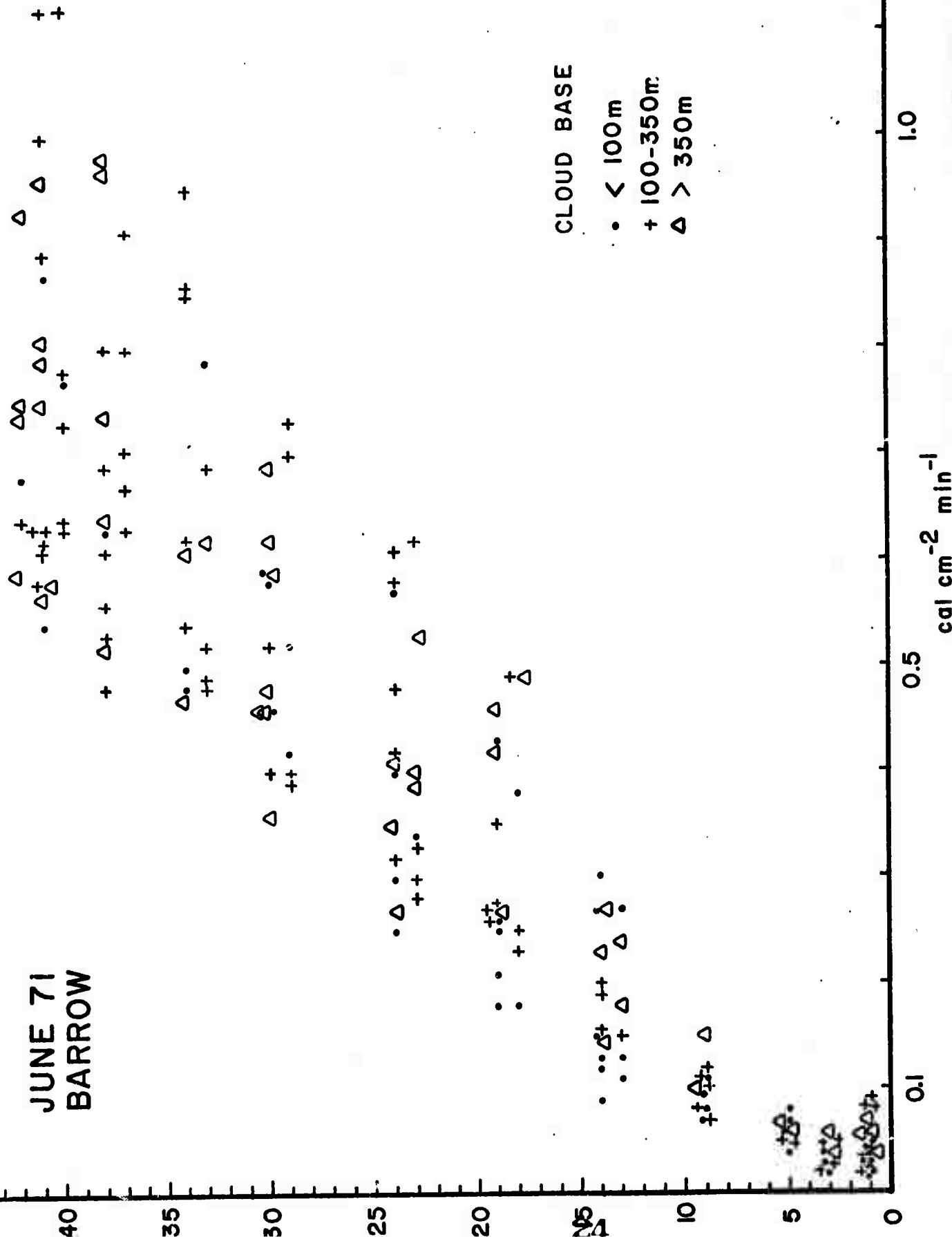
Figure 1. The incoming short wave radiation as a function of the solar elevation for three classes of cloud base height.
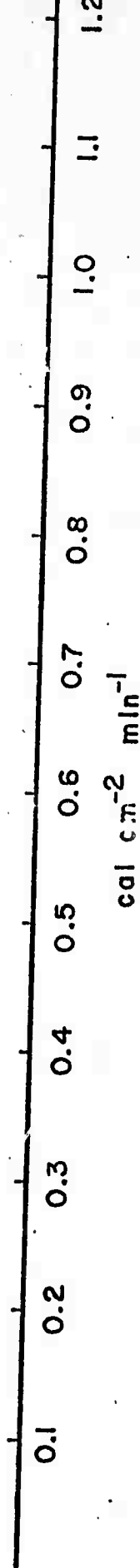
Figure 2. The incoming short wave radiation (mean values for solar elevation angles > 15° normalized to 30° solar elevation) as a function of the stratus cloud thickness. Each point represents a separate day of June 1971, Barrow, Alaska.

25

albedo d
absorption a

I_o

$(1-a) I_o d$

$a I_o$

$(1-a)^2 I_o (1-d)^2 \beta$

$a(1-a) I_o (1-d) \beta$

Cloud Layer

et.c.

$(1-a)^2 I_o (1-d) d \beta^2$

$(1-a)^2 I_o (1-d) d \beta$

$(1-a)^2 I_o (1-d) \beta$

$(1-a) I_o (1-d) \beta$

$I_o (1-a)(1-d)$

albedo β

$(1-a) I_o (1-d)(1-\beta) = $ absorbed $= (1-a)^2 I_o (1-d) d \beta (1-\beta)$
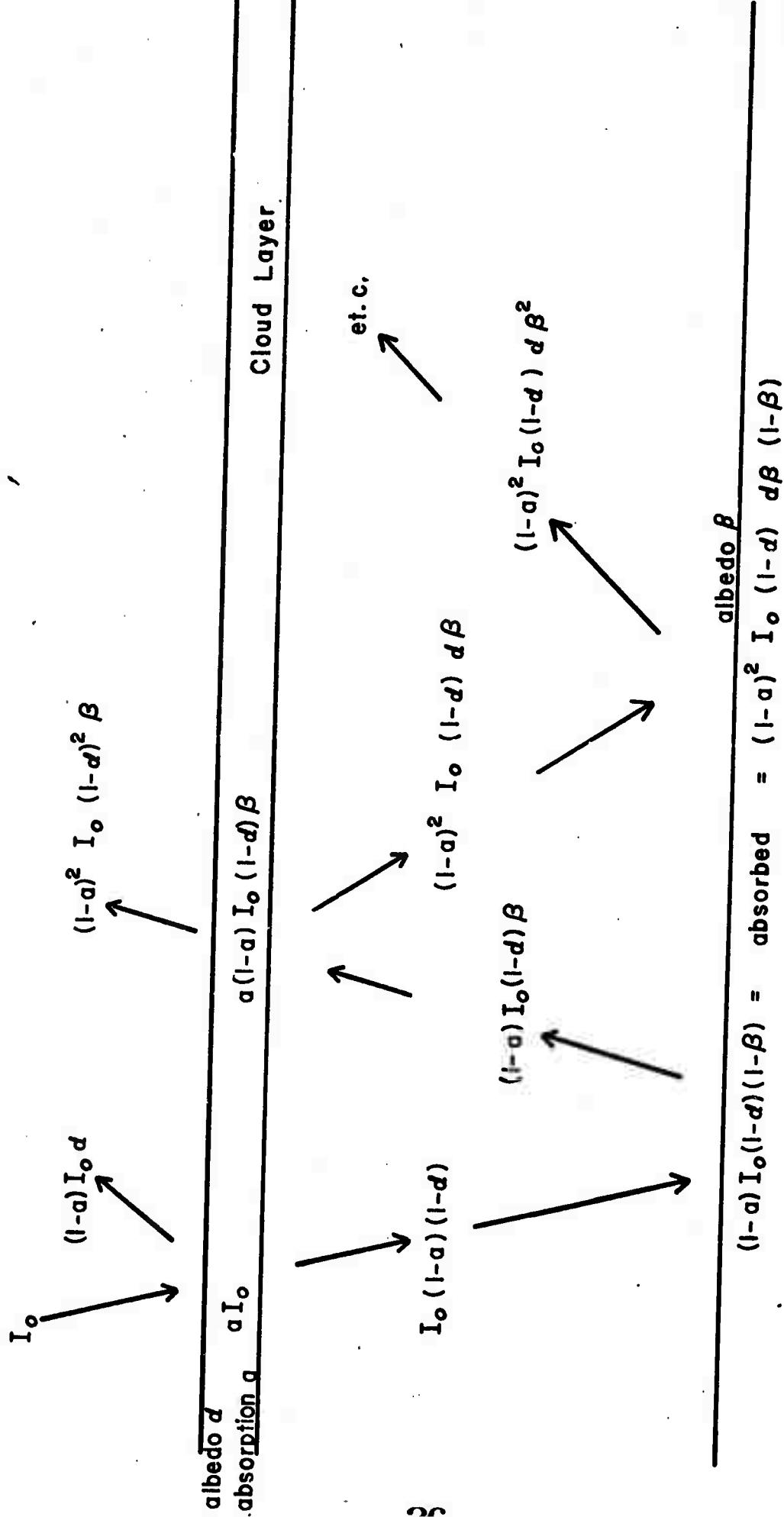
Fig 3 A simplified model of multiple reflection between a cloud layer and the surface.

with increasing cloud and surface albedo and with decreasing absorption in the cloud.

Calculations for the incoming radiation were carried out under the following simplifying conditions:

1) The incoming radiation on a cm^2 horizontal surface with a solar elevati n of 30° was estimated to be 0.80 cal cm^{-2} min^{-1}.

2) The albedo of the cloud was assumed to be 55% (this would be the albedo as seen if the cloud were above a black body).

3) The absorption in the cloud was assumed to be 7%.

Under these simplifying assumptions, the following values were found for three days, which had, according to the radiosonde ascents, similar cloud conditions:

1.	Date	2	10	29	June 71
2.	Hours	11	4	5	
3.	Surface albedo (measured)	79	58	20	%
4.	Incoming radiation (measured)	.56	.38	.26	cal cm^{-2} min^{-1}
5.	Mean solar angle	31	24	21	degree
6.	*Incoming radiation (measured)	.54	.47	.37	cal cm^{-2} min^{-1}
7.	*Incoming radiation (calculated)	.55	.44	.36	cal cm^{-2} min^{-1}

*Lines 6 and 7 were interpolated to 30° solar elevation.

One can see that the agreement between calculated and observed values are good. The decrease in incoming radiation of 32%, which was observed for similar cloud conditions between the beginning and end of June, can be explained solely by multiple reflection. At the beginning of June, the ground is covered with dry snow and the albedo is therefore high (around

27

80%), and multiple reflection is important. On June 10, the snow cover is melting, which lowered the reflectivity by about 20%, and decreases the importance of the multiple reflection. At the end of June, the snow cover is melted altogether and an albedo value of 20%, which was observed, is typical for the tundra surface. Now the multiple reflection is unimportant, which explains the decrease in the incoming radiation from 0.54 cal cm^{-2} min^{-1} on June 3 to 0.37 cal cm^{-2} min^{-1} on June 9. Theoretically, assuming the cloud conditions were identical, the decrease in the incoming radiation would have been expected to be even slightly larger (35%).

Summarizing, it has been shown by an example that multiple reflection is important in the Arctic. Therefore, it is not possible to give typical values of incoming radiation for a specific cloud type without knowing the conditions of the underlying surface. If one would, for example, calculate the radiation balance for an ice-free Arctic Ocean by using the observed incoming short wave radiation data obtained from ice islands, a serious error would be introduced.

However, more work has to be done in this direction. So far observational data of only 4 days were used. More radiation data with better cloud observations are needed. Also the model is too simple and should be improved.

III. COMPOSITION OF ARCTIC CLOUDS

K. Jayaweera and T Ohtake

Studies of the composition of arctic stratus clouds were made in two series of experiments at Barrow, Alaska; the first series was performed in September 1971 and the second in April 1972. The results of the initial experiments are now completed while the analysis is in progress for the second series.

The cloud particles were collected continuously in flight using an

28

MRI cloud particle sampler extending through the door of a Cessna 180 aircraft so that the sampling point is well outside the disturbed propeller wake (Figure 1). This instrument samples air at the rate of about 1.5 ℓ/sec at 100-knot flight speeds. A 4% solution of formvar in chloroform continuously coats a 16 mm clear leader film just before it exposes itself to the cloud-air through a small rectangular orifice. Permanent replicas of the cloud particles formed in the hardening formvar are later analyzed in the laboratory. We found film speeds of 4.5 inches per second during sampling the most satisfactory rate.

Clouds during September were rather typical of the summer and fall and consist entirely of stratus decks with weak or no updraughts. They usually are multi-layered, very often made up of two and sometimes three separate layers. Each of these cloud layers are about 1000 m thick and are usually separated from one another by a few hundred meters. We found clouds extending from nearly 200 m to over 4000 m above ground, hence we were able to sample clouds at temperature levels from +2 to -11C. Sampling was done by flying at a fixed height or constant temperature for about 5 minutes so that about 500 liters of air were sampled.

The ice crystal concentrations were determined by analyzing sections of at least 20 feet of film at a time, frame by frame, using a stop motion projector and counting the number of ice crystals within each section. The ice crystals were all columnar and unrimed. The concentrations of ice crystals at -11 and -7C were about 40 per m^3 and 10 per m^3, respectively, and at -4C it was less than 2 per m^3. These values are comparable to the ice nuclei concentrations at the corresponding temperatures measured by collecting air samples in a Millipore filter and developing them using the technique by Stevenson (1968) (Figure 2 and Section IV).
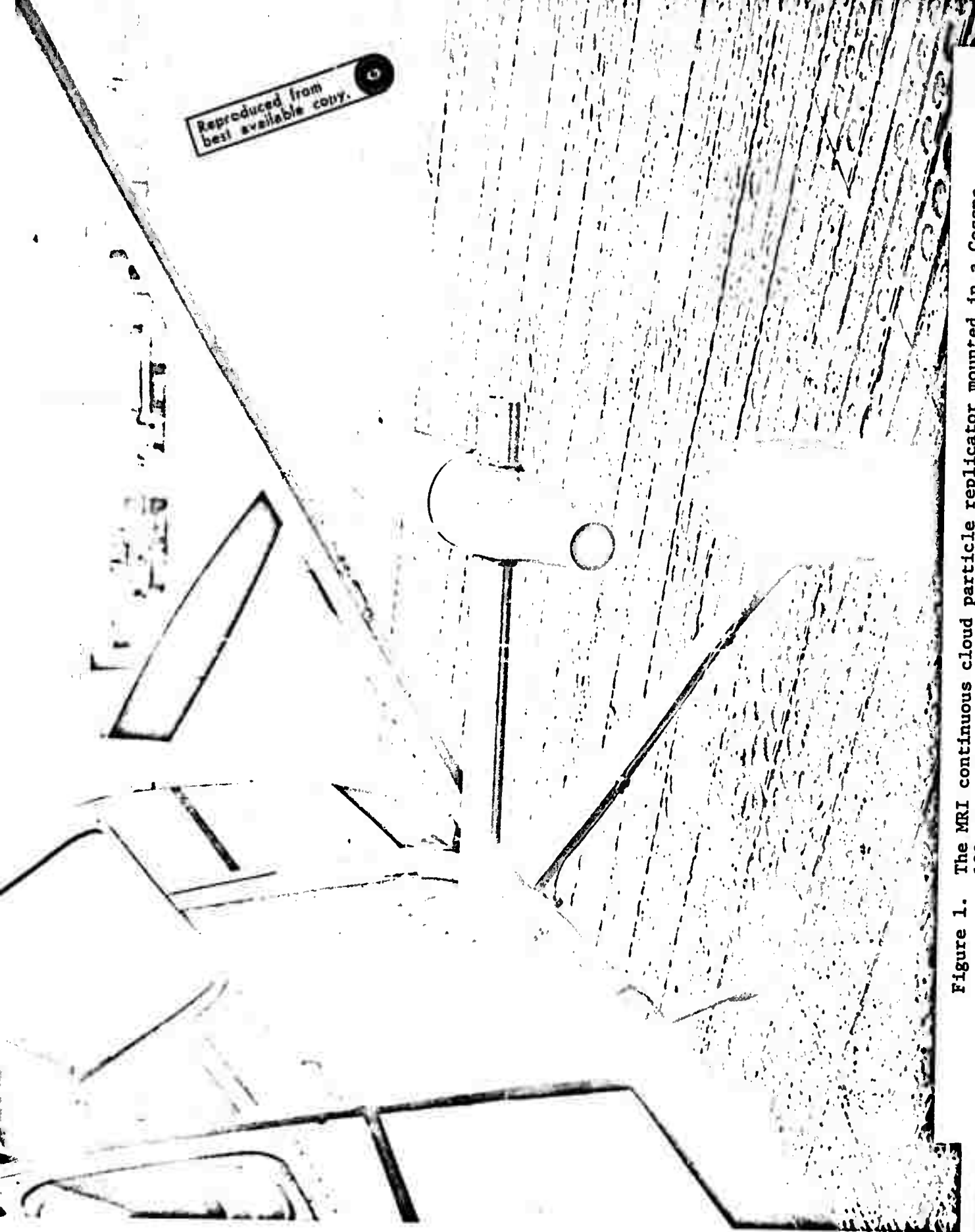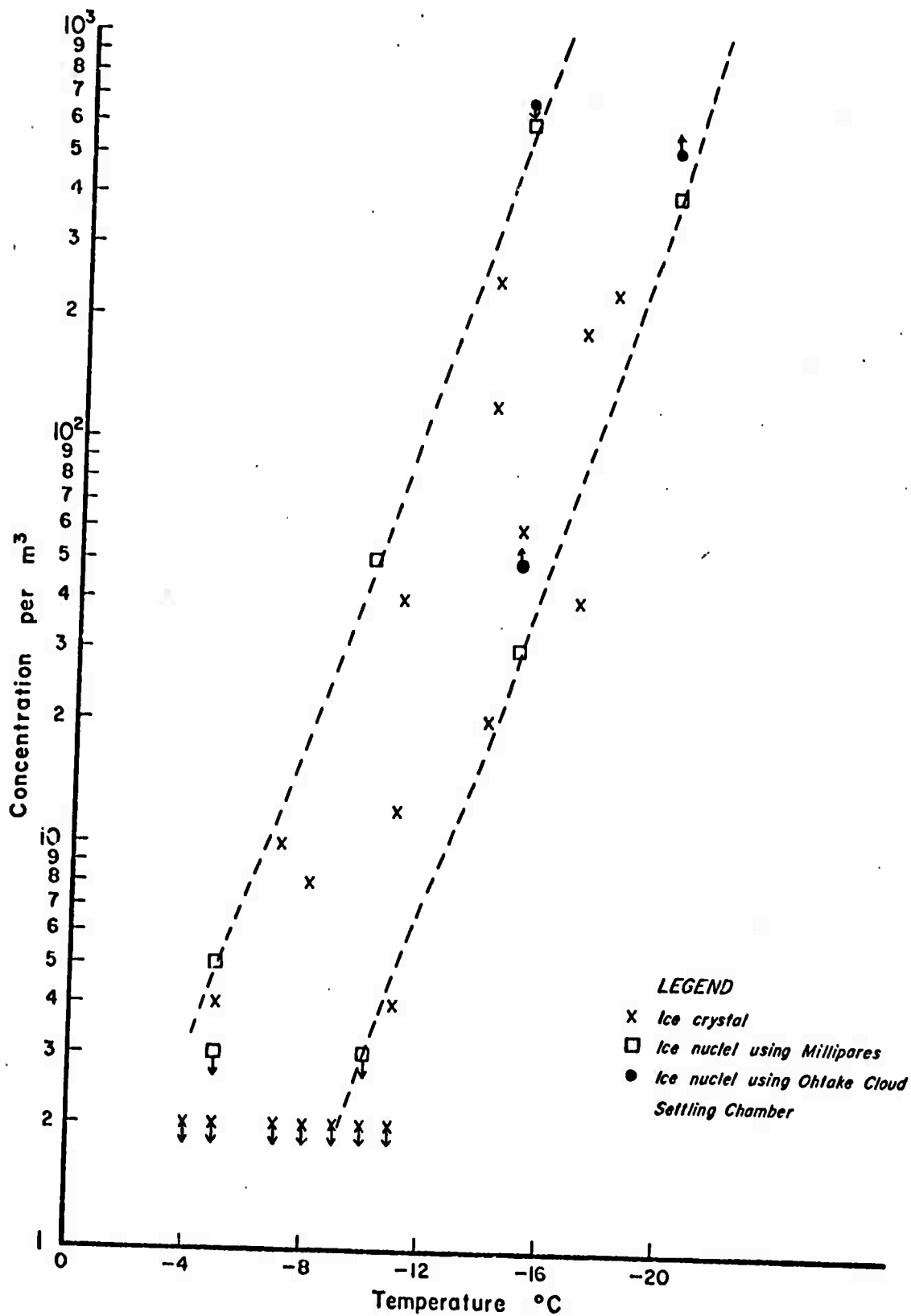
29

Figure 1. The MRI continuous cloud particle replicator mounted in a Cessna

30

Figure 2. Comparison of Ice Crystal Concentrations in Arctic Stratus and Ice Nuclei Concentrations (At Barrow, Alaska September 1971 and April 1972)

LEGEND
X   Ice crystal
□   Ice nuclei using Millipores
●   Ice nuclei using Ohtake Cloud Settling Chamber

The water droplet concentration and size distribution were determined by photographing, at one foot intervals, the formvar replicas under a microscope. One such photograph is shown in Figure 3. The concentration of the droplets averaged about 90 per cm^3 at all levels. It must be mentioned, however, that the concentration varied through the cloud, owing to the patchy nature of the latter, from almost zero to about 150 per cm^3. The l.w.c. was about 0.2 gm m^{-3}. The size distribution did not show significant variation at different levels, hence the overall size distribution for all the levels is shown in Figure 4. This, of course, was corrected for the droplet spread and collection efficiency of the droplets. The 3 μm cutoff is a result of the zero collection efficiency of the sampler for droplets below this size.

IV. ICE NUCLEI CONCENTRATIONS IN THE ARCTIC REGION

T. Ohtake and K. Jayaweera

Ice nuclei are necessary particles to form ice crystals in the atmosphere. Normally, these are not present in abundant quantities compared to condensation nuclei. To initiate precipitation in cold regions, ice crystals should be present in supercooled water clouds, even in small quantities, hence it is important to know the concentration of ice nuclei. In arctic regions occasional snowfalls occur even in summer and further research into global mechanisms for the influx of fresh ice nuclei from other regions through either the lower or upper atmosphere is needed. The importance of ice crystal aerosols on the arctic radiation regime has been pointed out by Fletcher (1966).

During April 1972, concentrations of ice nuclei were observed at Barrow, Alaska, by the following two methods:

16

$d_{mode} = 13.5 \,\mu m$
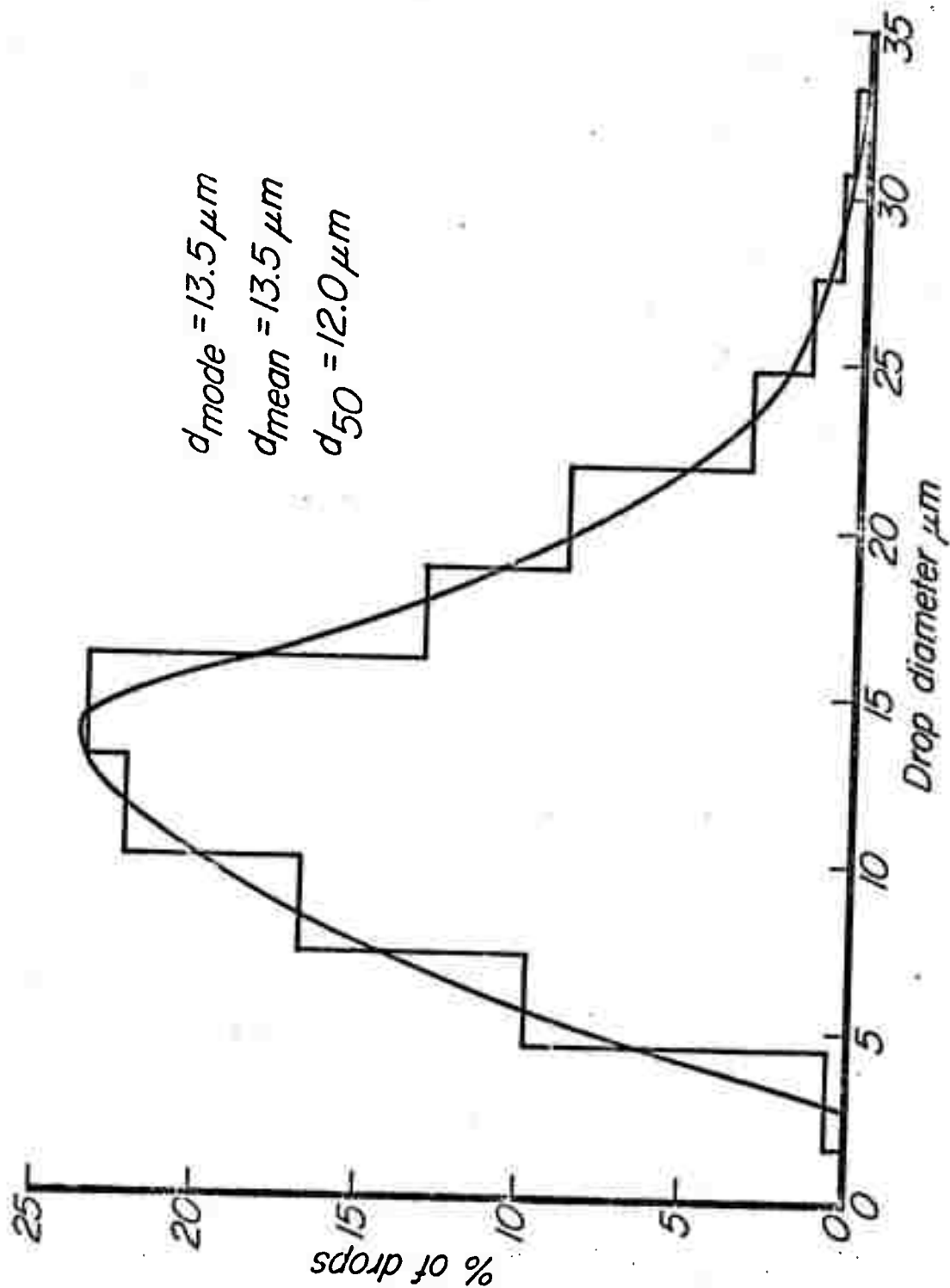
$d_{mean} = 13.5 \,\mu m$

$d_{50} = 12.0 \,\mu m$

Figure 4. Mass and number distribution of Arctic stratus clouds at Barrow.

1) Cloud-settling chamber of ice nuclei counting (Ohtake, 1971). Outside air was introduced into the 10 ℓ chamber using a vacuum pump. After the air is cooled to a desired temperature (-15°C or -20°C), supercooled cloud droplets are introduced into the chamber to give water saturation exactly the same as that in natural clouds. If any ice nuclei exist in the chamber, these will changed to ice crystals, which will then fall into a supercooled sugar solution and grow to visible size. The number counted will be the number of ice nuclei in the 10 liters of air. Figure 1 shows all the data we observed at -15°C and -20°C; they are compared with concentrations of ice crystals in the atmosphere (see section on cloud composition).

2) Millipore filter method. The air containing ice nuclei was drawn in through two Millipore filters once daily; volumes sampled were 250 liters and 360 liters. The filters are developed in a manner similar to that of Stevenson (1968) in a processor at the laboratory in the Geophysical Institute, as follows:

The filters are cooled to -20°C and are subjected to various amounts of moisture in the processor for 20 minutes. The number of ice crystals formed on a filter indicates the number of nuclei of the sample volume. This analysis is in progress now.

A postulate for a transport mechanism for ice nuclei will possibly emerge after all the data are analyzed. The comparison of data obtained by the cloud-settling method and the Millipore filter method will be valuable, particularly if compared further with the measured concentrations of ice crystals and ice nuclei in the undisturbed polar air, because of complications in the measuring techniques concerned with ice nuclei concentration (Bigg, 1970).

Condensation nuclei concentrations were observed in addition to measuring the ice nuclei concentrations. Condensation nuclei counts consistently
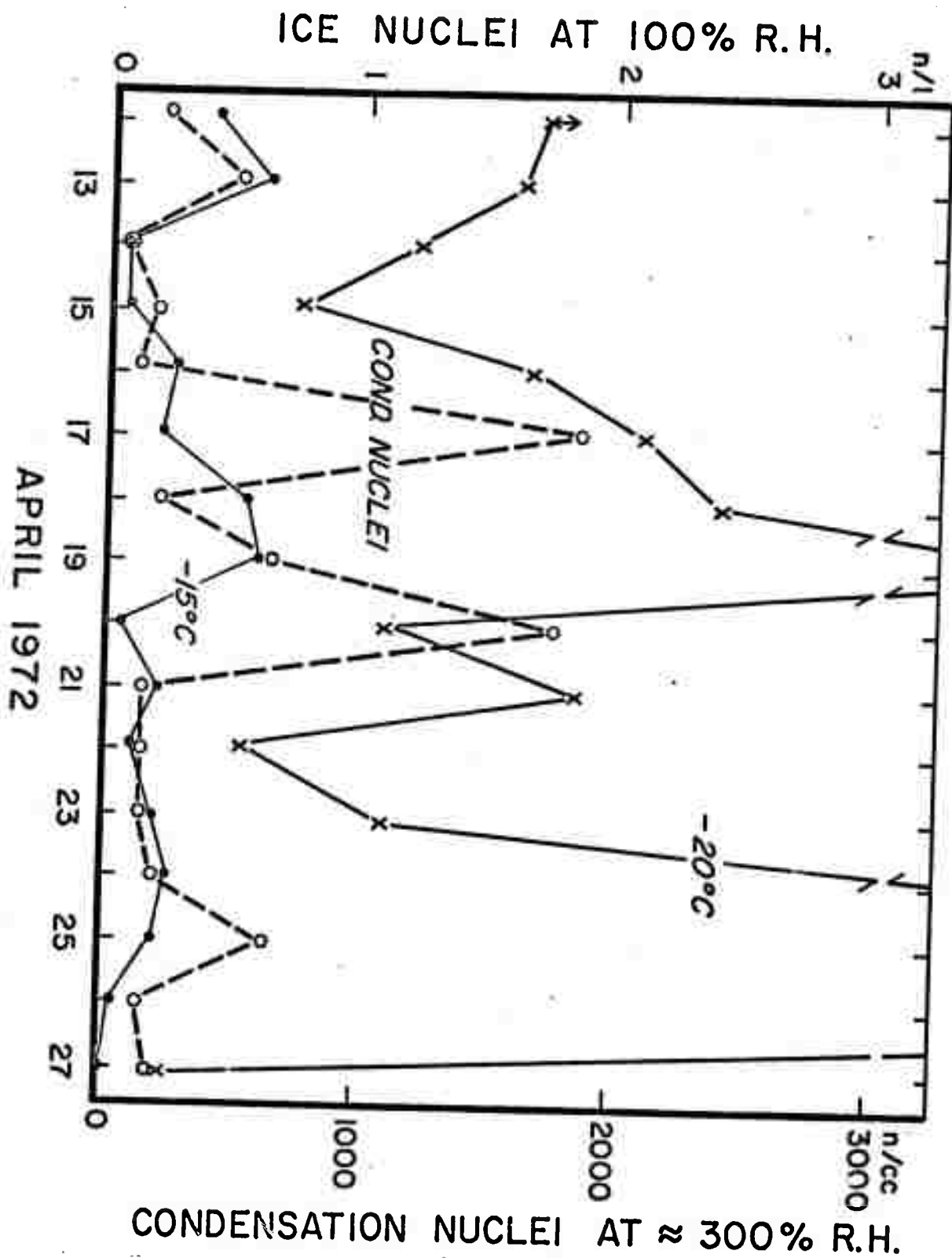
35

Figure 1. Concentrations of ice nuclei effective at -15°C and -20°C
and condensation nuclei (Aitken nuclei) t Barrow, Alaska.
Note that the concentrations of ice nuclei at -15° and -20°C

increased when winds shifted to directions from inhabited areas, even though absolute numbers in unit volume of air were quite small compared with other areas in Alaska. On the other hand, ice nuclei concentrations were unaffected by winds from inhabited areas. It is suggested that these two types of nuclei have different origins.

Summarizing the results, we could say that the non-precipitating stratus clouds over the arctic, within this temperature range, have a narrow droplet spectrum typical of stratus clouds. Ice crystal concentrations are low and can be predicted from the ice nuclei concentration.

In the April 1972 experiments, the clouds were again stratus, except on one occasion, when strato-cumulus was observed. On two occasions the sampling was done in a cloud which was producing snow on the ground. The cloud temperatures were lower than in the previous experiments, with the lowest sampling temperature being -15C. Preliminary analysis indicates that the concentration of water drops is considerable and the concentration of ice crystals is higher and corresponds to that expected from ice nuclei concentrations (100 per m^3 at -15C). In these temperature regions the ice crystals are plate-like and dendritic. Even though we used a decelerator to reduce the air speed to one-half the aircraft speed, the dendritic crystals were all found to have shattered on impact. The pieces of the shattered ice crystals were found in clusters on the film. However, solid hexagonal plates were found intact. Analyses are now in progress to determine the concentration of ice crystals and the size distribution and concentration of water droplets.

37

V. ABSORPTION AND SCATTERING BY ATMOSPHERIC AEROSOLS

G. Shaw

Direct solar radiation was experimentally monitored at several discreet wavelength intervals in the visible part of the solar spectrum, and as a function of altitude with an airborne radiometer. The major scientific objective was to determine the height and wavelength distribution of the optical extinction coefficient, $\beta(h,\lambda)$, arising from absorption and scattering from atmospheric aerosols over a location in the arctic basin. Data were accumulated near Barrow, Alaska, to an altitude of 5000 meters during the month of April 1972. Supplementary measurements were made on a Convair 990 aircraft that flew north from Fairbanks to latitude 76°N. These Convair flights extended the measuring altitude to 11 km. This report summarizes initial results; the theory, instrumentation, calibration, and experimental procedure are outlined in Appendix I.

38

The aerosol extinction coefficient, $\beta_D(\lambda, h)$, was obtained by the analysis techniques described in Appendix I. At the time of this writing all data have not been completely analyzed; however, some preliminary results from two selected flights are available and will be presented in this section.

Flight Number 4

Figure 1 shows the analog record obtained during flight number 4 on April 8, 1972, extending from times 2025 to 2127 GMT. The sky was completely clear, ground temperature was -22.5°C and visibility about 20 miles. The flight azimuth was held at 110°, climb rate was adjusted to 500 ft/min to a maximum altitude of 10,000 ft, filter at 5000 Å was used. After leveling off at 10,000 ft, the aircraft descended at a rate of 400 ft/min to an altitude of approximately 50 ft; during the descent phase the 7000 Å filter was used. The data acquisition ceased at a distance of 85 miles from Barrow. (Unfortunately, data could not be taken during the return flight because of the geometry imposed by the aircraft and radiometer part.) The solar elevation ranged from 25.7° to 23.6° during this flight.

Figure 2 illustrates the aerosol extinction coefficient at $\lambda = 5000$ Angstroms as determined by the analysis method described in Appendix I section. Plotted adjacent to the optical extinction coefficient is the temperature profile. The radiative inversion extended to a height of 2000 ft with an average lapse rate of +34.0 °C/kms; thereafter, a roughly isothermal region extends to about 6000 ft elevation after which the lapse rate approached the moist adiabatic value of -6°C/km for higher altitudes. There is some slight structure in the temperature curve with a relative maximum (warm region) near 3000 ft. The optical
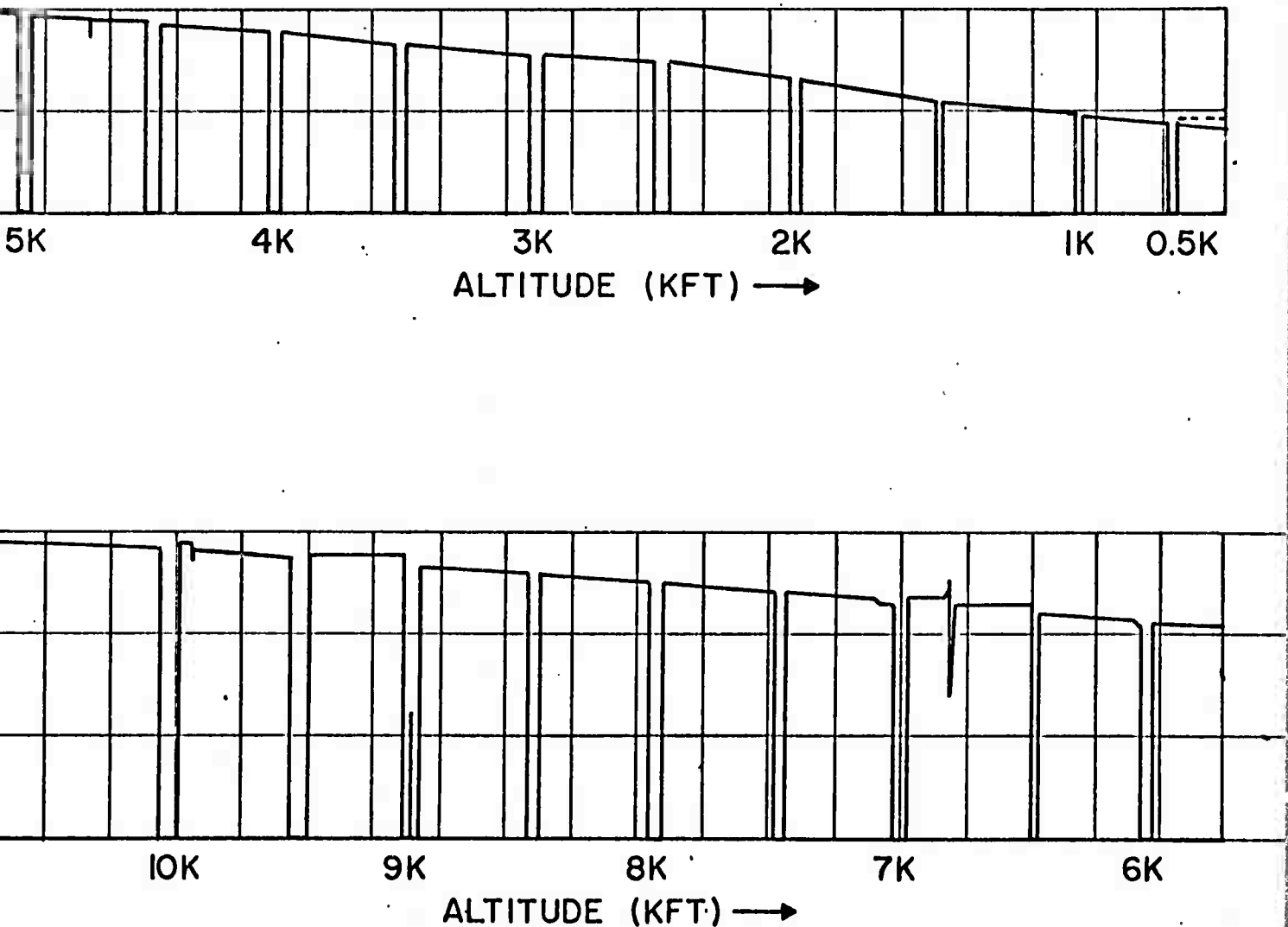
39

FLIGHT NO. 4
BARROW, ALASKA
APRIL 8, 1972

Figure 1. Analog record of radiometer output voltage (proportional to the solar intensity at 5000 Å) obtained during flight number 4.
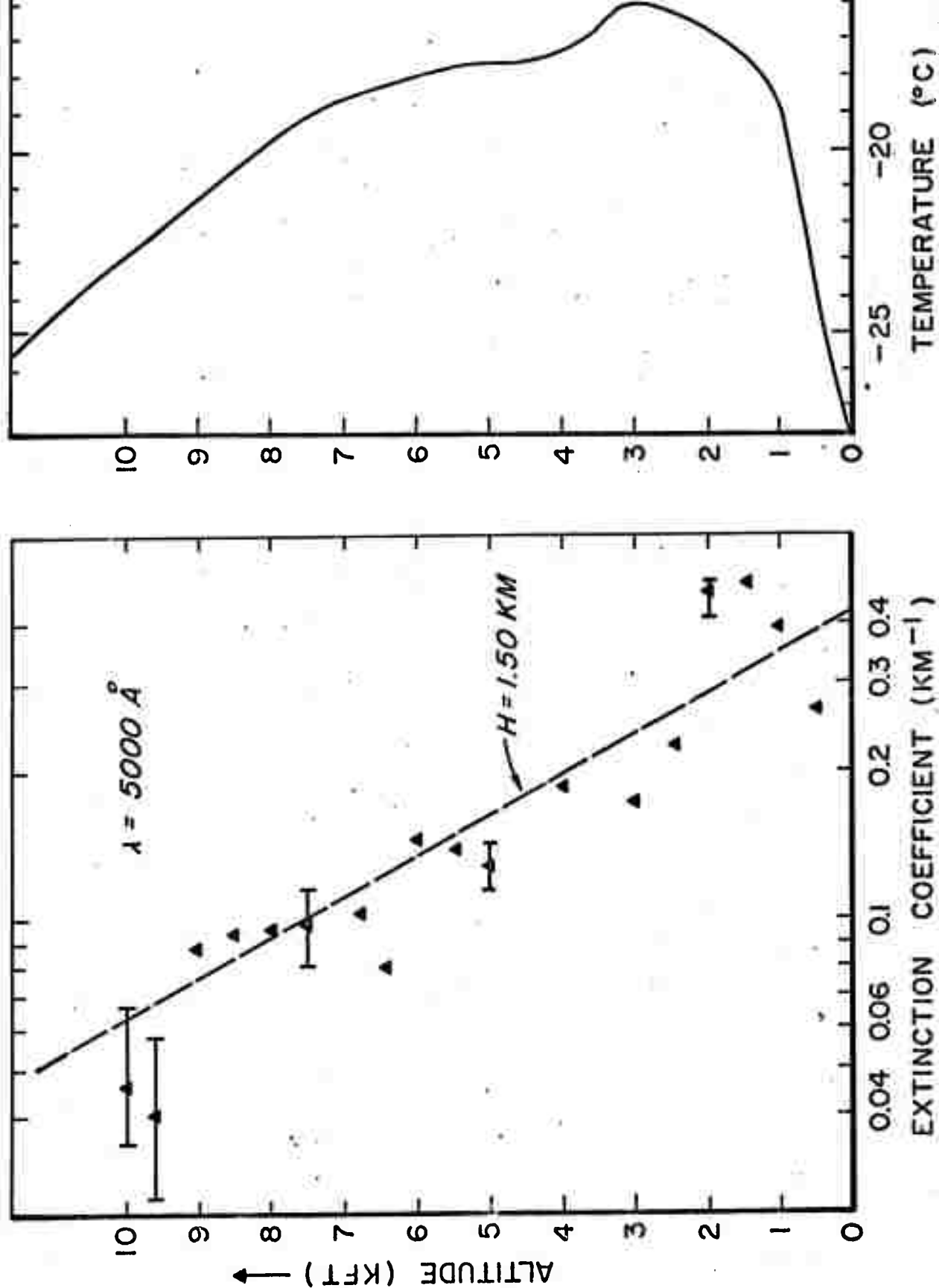
Figure 2. Optical extinction coefficient, β(h,5000), and temperature profile obtained during flight number 4 on April 8, 1972 near Barrow, Alaska.

41

extinction coefficient, $\beta(h,5000 \overset{o}{A})$, shows a general decrease with altitude. The individual points have rather considerable scatter which are mainly carried by error in reading the slope of the $I(\lambda,h)$ vs h curve. The <u>tendency</u> for the extinction coefficient to peak near 1500 ft altitude seems to be real; other short periodicities are probably noise and can be averaged out. A line drawn through the data points gives an approximate empirical expression for $\beta(h,5000 \overset{o}{A})$ as

$$\beta(h) = 0.410 \ e^{-\frac{h}{H}} \tag{1}$$

$$H = \text{aerosol scale height} = 1.50 \text{ km}$$

The total optical depth (at 5000 $\overset{o}{A}$) can be obtained from eq. 4 (Appendix I) and, at the maximum altitude of 10,000 ft is found to have a numerical value of 0.231. Subtraction of the optical depth arising from molecular scattering above 10,000 ft ($\tau_R = 0.099$) and optical depth arising from ozone absorption ($\tau_G = 0.014$) yields an optical depth of 0.117 above 10,000 ft elevation.

Atmospheric aerosols are distributed in two height regions, namely in the lower troposphere and also within the stratosphere. The aerosols in the stratosphere may give rise to the majority of the extinction above 10,000 ft. To estimate the magnitude of the extinction caused by the stratospheric aerosols we assume that the troposphere extinction coefficient can be estimated for heights greater than 10 kft by extrapolating the exponential relationship given by eq. 1. Thus, the total aerosol depth above 10,000 ft (2.94 km) arising from the exponential decrease of tropospheric aerosol is

$$\tau(h>10 \text{ kft}) = \int_{2.94}^{\infty} 0.41 \ e^{-h/H} \ oh = 0.092 \tag{2}$$

Therefore, the residual optical depth attributable to extinction by

the stratospheric aerosol would be $\tau_{strat} = 0.117 = 0.092 = 0.025$.

Admittedly, the above method for estimating the extinction arising from stratospheric aerosol is, at best, somewhat crude and almost certainly the height profile of the optical extinction coefficient is complex and cannot be well represented by extrapolation of the lower level extinction coefficient. However, the method is plausible and offers a rough way to deduce the stratospheric extinction.

The most noteworthy point about the atmospheric optical parameter as inferred by the data accumulated on flight 4 is the unexpected high values for atmospheric turbidity. The data yields a total value of optical depth equal to .670 for a wavelength of 5000 $\overset{o}{A}$ and at ground level. After subtracting out Rayleigh and ozone absorption one is left with $\tau_D = .510$. This value is to be compared with a standard mid-latitude atmosphere tabulated by Elterman (1968) who gives a value of $\tau_D = 0.264$. Moreover, the high value of optical depth found at Barrow is completely at odds with actinometric data acquired during the spring and summer of 1970 and 1971 at McCall Glacier (69°18'N, 143°48'W) in northeast Alaska where an average value of $\overset{o}{A}$ngstrom turbidity coefficient was found to be approximately 0.020 (Shaw and Wendler, 1972) which corresponds to an optical depth due to dust at $\lambda = 5000$ $\overset{o}{A}$ of 0.049 (assuming a $\lambda^{-1.3}$ wavelength dependency). At an altitude of 1700 meters corresponding to McCall Glacier our measured aerosol optical depth, τ_D, was 0.220 or a factor of 4.5 larger than the background level as recorded at McCall.

Inspection of other data acquired during April shows that the optical depth obtained during flight 4 was unusually large. The reason for this particularly large value of aerosol optical depth is unknown.

<center>**43**</center>

However, some clue to the cause may be found by inspecting the synoptic maps. Figure 3 shows the synoptic situation at the surface, at the 850 mb level and at the 500 mb level during flight number 4. By inspecting previous maps and by comparing the temperature profile trend, it was determined that a cold polar air mass had recently been intruded by a relatively warm continental southerly flow. In particular, the circulation near the surface was from 160° azimuth from interior Alaska. At higher levels the winds veered to clockwise to 290° at 850 mb, and about 10° at 500 mb. It is conceivable that the high turbidity had its origin, at least in part, because of the low southerly flow paths over interior Alaska. During the period of measurement the ground was exposed to the south of the Brooks Range in northern Alaska and, hence, it is possible that the large dust content could have originated from interior and southern Alaska.

The high turbidity during flight 4 could also be partly due to sub-visible cirrus ice clouds associated with the strong low pressure system centered at some 400 miles to the southwest of Barrow. As the flight progressed toward a bearing of 80° true the airplane would move further away from the low pressure system and thus may encounter clearer air. This seemed to be the case as indicated by a record of solar intensity obtained while flying at constant elevation. Thus, the large apparent turbidity may be due partly to ice crystals in the thin cirrus clouds.

Flight Number 5

Flight number 5 occurred on April 10, 1972 from 1422 to 1553 AST. Sky conditions were clear; visibility approximately 50 miles; wind ENE at 15 knots; ground temperature -17°C. After gaining altitude and
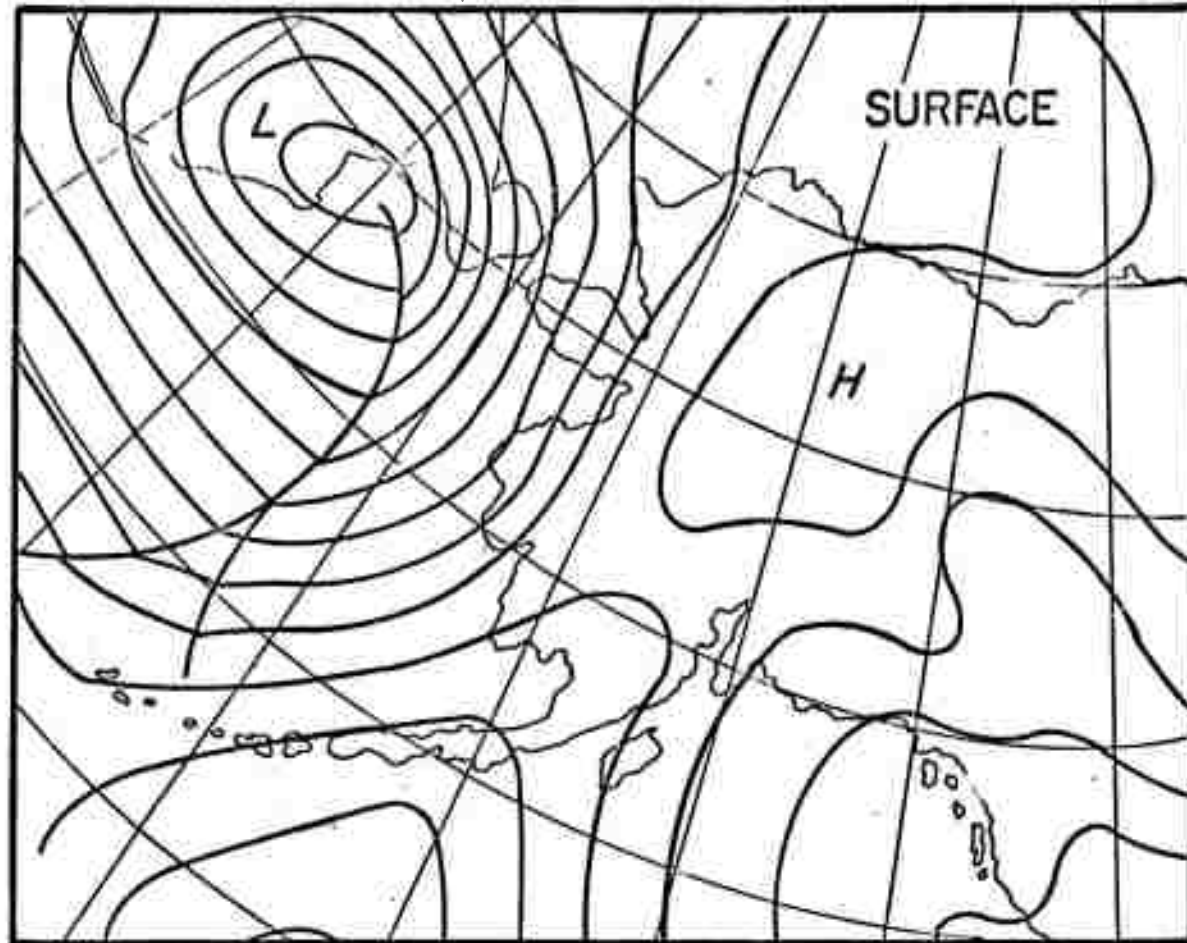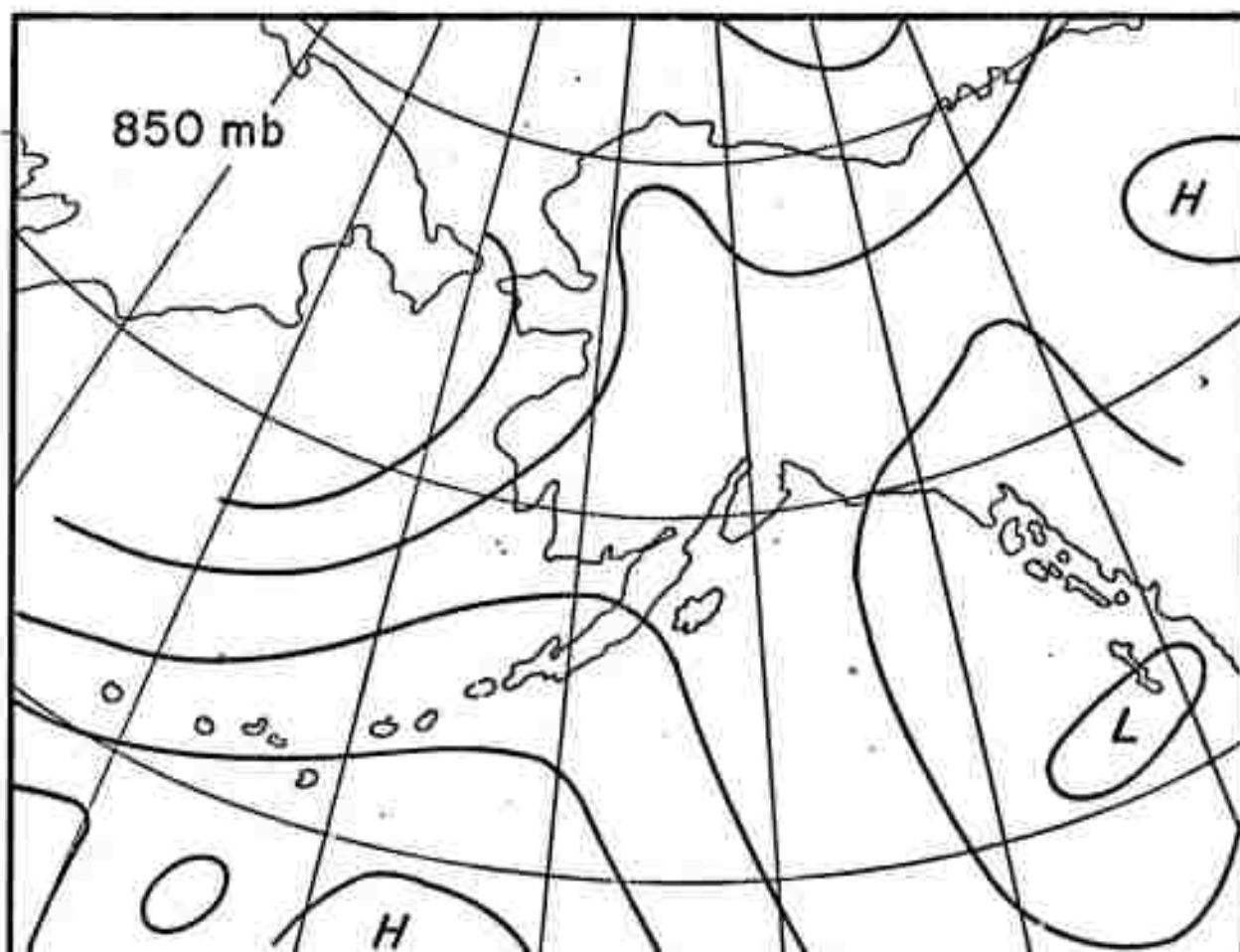
44

Figure 3. Synoptic situation at (a) surface; (b) 850 mb level; and (c) 500 mb level, for the vicinity of Barrow during the time period of flight number 4.

45

carefully scanning the sky some very tenuous cirrus were visible near the azimuth of the sun but considerably below the sun. The solar elevation angle during the flight varied from 23.5° to 19°.

Optical data were accumulated at 5000 Å and at 7000 Å. Evidence of horizontal inhomogeneities encountered during the acquisition of the data at 7000 Å render its value somewhat questionable. However, the data acquired at 5000 Å during both ascent and descent seem to be consistent and thus these data will be discussed.

The extinction coefficient arising from aerosols at 5000 Å is shown in Figure 4. Although there is a considerable scatter in the individual data points, the trend of decreasing volume extinction with increasing altitude is quite apparent. A straight line fit through the data yields a scale height of 1.1 km which is somewhat smaller than the scale height found one day earlier during flight number 4.

The aerosol optical depth evaluated at 5000 Angstroms at the ground and at peak altitude are as follows

τ_D = 0.280 at ground level

τ_D = 0.062 above 12,000 ft (3.52 km)

The values above are about half of the corresponding values found the previous day during flight number 4. There is some tendency for the aerosols to be trapped where the temperature structure is concave to the right; however, the inherent scatter of the individual points makes any definite inferrence somewhat difficult. Again, the scatter of the points is mostly caused from errors in reading dI/dh from the analog record - the process is statistically unbiased, however, and the average trends are meaningful. The large variance in individual points is basically due to noise added by the process of differentiation.

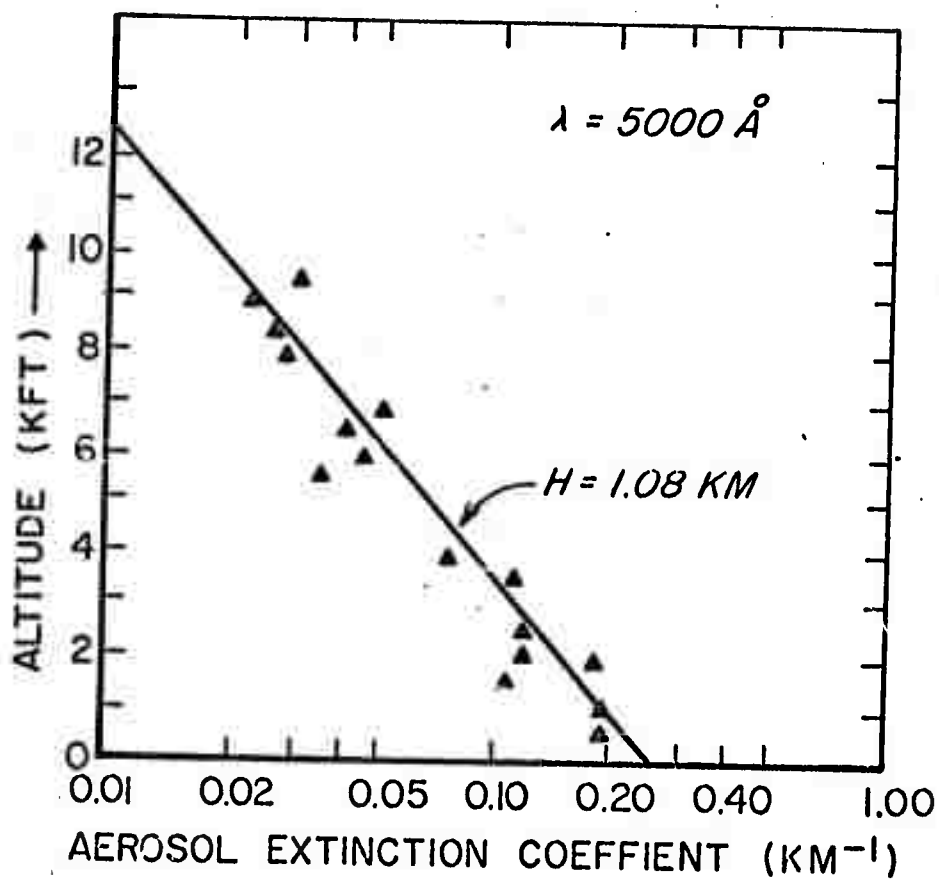FLIGHT NO. 5

$\lambda = 5000 \overset{\circ}{A}$

$H = 1.08$ KM

ALTITUDE (KFT)

AEROSOL EXTINCTION COEFFIENT (KM⁻¹)

Figure 4. Optical extinction coefficient, $\beta(5000,h)$ obtained during flight number 5 on April 10, 1972 near Barrow, Alaska

47

The residual optical depth above 12,000 ft (3.52 km) is probably at least partially caused by the optical extinction by the stratospheric aerosols. Assuming the continuation of the exponential dependency of $\beta(h)$ to heights above 3.5 km would yield an optical depth equal to 0.012 above 3.5 km. Thus, it would be inferred that τ_D stratosphere = 0.062 - 0.012 = 0.050. It becomes very difficult to accurately assess optical depths of this small magnitude and, in fact, an error analysis shows that the residual stratospheric extinction is subject to an error of the order of $\tau_{D_{strat}}$ = 0.050 $\pm$ 0.025.

Convair 990 Flights

Data from the Convair 990 flights have not at the time of this writing been subjected to analysis. Briefly, two flights were made, both originating from Eielson Air Force Base and flying to a grid near the AIDJEX campsite. The flights extended to 76°N latitude and encompassed an altitude range from 40 ft msl to 37,000 ft (10.8 km).

The optical measurements were made at 7000 $\overset{o}{A}$ and at 5000 $\overset{o}{A}$ through one inch thick plexiglass ports with vertical angle of +14°. Unfortunately, a great deal of flying time was spent either flying almost into or out of the solar azimuth and, since data could only be accumulated at times when the sun was at nearly right to the aircraft bearing, only a limited amount of data were accumulated. However, these measurements that were obtained upon cursory inspection seem to be of good quality and most likely will provide more useful information, especially in regards to the stratospheric aerosol extinction.

SUMMARY

The airborne method of studying the vertical distribution of atmospheric aerosols has provided a considerable amount of valuable information. The optical extinction coefficient is found to vary in the

48

troposphere in an approximately exponential fashion with a scale height of the order of 1 to 2 km; these numerical values are in reasonable agreement with previous inferences from lidar and searchlight methods (Elterman, 1968).

The high value of atmospheric turbidity near Barrow is difficult to explain, especially in April when the ground is still frozen. Pack ice covered the ocean surface at the time of data accumulation; however, there was an open lead several miles offshore and occasionally a fog could be seen to emanate from the lead and spread for one or two kilometers downwind. We feel that the ice cloud seeded by this lead was not responsible for the high optical depths because, for example, during flight number 4 the wind was from a southerly direction which would tend to blow the fog away from our observing site.

Additional analysis of existing data and the acquisition of more optical depth information at Barrow will perhaps delineate the cause of the unexpectedly large values for atmospheric optical depths.

VI. THEORETICAL ASPECTS OF RADIATIVE TRANSFER IN THE ARCTIC ATMOSPHERE

S. A. Bowling

Introduction

Some work was carried out during the year on several theoretical aspects of radiative transfer in the arctic atmosphere. An infrared transfer model previously developed for ice fog (Bowling, 1970) was expanded to allow for a clear air layer below a cloud deck. In addition, improvements were made in the temperature-dependence of the model. Using a model and a measured size distribution for arctic stratus clouds (Section III), atmospheric cooling rates with and without the cloud deck were computed. In addition, an

49

approach has been developed which allows computation of fluxes in an atmosphere with several cloud layers. Programming on this model is in progress. Finally, some rough calculations have been made on the effect of a thin, purely scattering cloud layer on the total energy absorption of the earth-atmosphere system at various latitudes and seasons.

3-Layer Model

The 3-layer model as it currently exists allows for two clear air layers with an absorbing and scattering layer sandwiched between them. Carbon dioxide and water vapor are accounted for throughout the 29-point sounding, and ozone is considered to provide an upper-boundary input in the 10 µm region. A temperature discontinuity at the ground is allowed, as is a wavelength-dependent ground albedo, but neither of these features has been utilized to date. Cloud absorption and scattering cross-sections, as well as generalized absorption coefficients for water vapor and carbon dioxide, are specified over 63 wavenumber intervals. Interval widths are 40 cm^{-1} over most of the spectrum, with 10 cm^{-1} resolution over the CO_2 band and 200 cm^{-1} bandwidth on the shortwave side of 1600 cm^{-1}. Variation of gaseous absorption parameters with temperature is handled by Elsasser's (1960) parabolic correction, assuming the temperature is the mean temperature of the total absorption path under consideration. The absolute accuracy is probably comparable to that of Elsasser's tables as corrected by Zdunkowski et al. (1966); the difference between calculations with and without clouds is probably better than this. Calculation of fluxes and cooling rates over the 29 sounding intervals requires less than 5 minutes of CDC 7600 computer time.

A standard Mie scattering coefficient program available at the National Center for Atmospheric Research has been modified to accept complex refractive indices for the 63 wave numbers used in the radiation program and any

50

measured or theoretical size distribution, to calculate the absorption and flux backscatter coefficients, and to punch the results on cards in a format suitable for direct inclusion in the radiative transfer program. A measured size distribution for arctic stratus clouds (Section III) was combined with the complex refractive index for water given by Irvine and Pollack (1968) in this Mie program. The results are shown in Figure 1. An August sounding from Point Barrow was then used to calculate cooling rates with and without this cloud, the cloud height and depth being determined by the saturated layers in the original sounding. Latent heat effects were included in calculating the cooling rates. Results are shown in Tables 1-3. Flux values are in cal/(cm^2 12 hours) and cooling rates in °C/12 hours.

In general, the results confirm a tendency noted in every computation made thus far. The rate of energy loss decreases at the ground, from the atmosphere below the cloud, and from the earth-atmosphere system as a whole (assuming the cloud temperature is below that of the ground). Cooling rates above the cloud are enhanced, and the cloud itself may show increased cooling rates (for low clouds and/or low surface temperatures) or heating (for high, cold clouds over warm surfaces). The first case is probably always true for arctic stratus.

Visible Radiation

A very simple model of the effects on solar radiation of a thin cloud was developed. The model included multiple reflections between cloud and surface, and integrated solar angle over a 24-hour day. Cloud particles were assumed to be pure scatterers and a single scattering event (from a cloud particle or the surface of the earth) was assumed to destroy all directional characteristics of the incoming radiation. The albedo of the underlying surface was assumed independent of solar zenith angle. The model
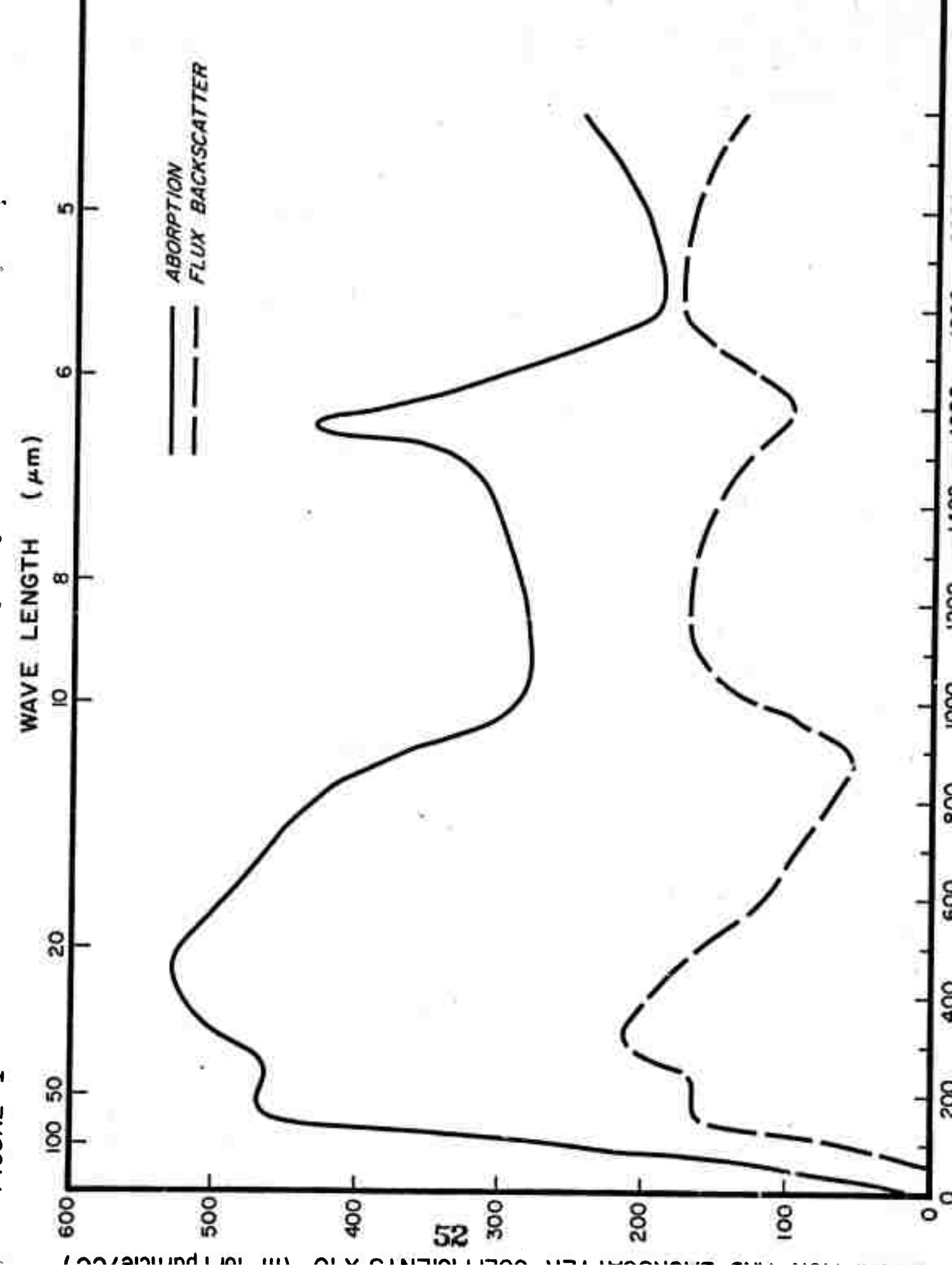
FLUXES AND HEATING RATES

Z,M.	T,C	FLUX	LAYER LIMITS			FLUX DIV.	HEATING
0.0	1.7	84.791	0.0M.	TO	100.0M.	.006	-.201
100.0	2.4	85.407	100.0M.	TO	200.0M.	.015	-.483
200.0	3.1	86.863	200.0M.	TO	299.0M.	.028	-.927
299.0	3.8	89.590	299.0M.	TO	551.0M.	.024	-.817
551.0	2.6	95.591	551.0M.	TO	988.0M.	.011	-.403
988.0	.3	100.544	988.0M.	TO	1051.0M.	.014	-.521
1051.0	1.7	101.438	1051.0M.	TO	1875.0M.	.019	-.725
1875.0	-.6	116.905	1875.0M.	TO	2587.0M.	.020	-.822
2587.0	-4.5	130.823	2587.0M.	TO	4304.0M.	.012	-.589
4304.0	-17.0	152.125	4304.0M.	TO	4921.0M.	.013	-.701
4921.0	-23.1	160.191	4921.0M.	TO	5044.0M.	.018	-.974
5044.0	-23.8	162.344	5044.0M.	TO	5168.0M.	.025	-1.437
5168.0	-24.9	165.505	5168.0M.	TO	6855.0M.	.003	-.185
6855.0	-37.5	170.549	6855.0M.	TO	7575.0M.	.001	-.060
7575.0	-40.0	169.947	7575.0M.	TO	7779.0M.	-.000	.018
7779.0	-41.3	169.900	7779.0M.	TO	26500.0M.	.004	.541
26500.0	-43.9	240.123					

TABLE 1

August 11, 1970, 1200Z, No Clouds

53

29

FLUXES AND HEATING RATES

Z.M.	T.C	FLUX	LAYER LIMITS	FLUX DIV.	HEATING
0.0	1.7	-4.894	0.0M. TO 100.0M.	-.005	.175
100.0	2.4	-5.429	100.0M. TO 200.0M.	.001	-.021
200.0	3.1	-5.366	200.0M. TO 299.0M.	.011	-.382
299.0	3.8	-4.242	299.0M. TO 551.0M.	.026	-.504
551.0	2.6	2.419	551.0M. TO 988.0M.	.022	-.455
988.0	.3	12.051	988.0M. TO 1051.0M.	1.229	-24.906
1051.0	1.7	89.485	1051.0M. TO 1875.0M.	.022	-.831
1875.0	-.6	107.213	1875.0M. TO 2587.0M.	.020	-.840
2587.0	-4.5	121.436	2587.0M. TO 4304.0M.	.012	-.592
4304.0	-17.0	142.869	4304.0M. TO 4921.0M.	.013	-.699
4921.0	-23.1	150.917	4921.0M. TO 5044.0M.	.017	-.972
5044.0	-23.8	153.065	5044.0M. TO 5168.0M.	.025	-1.435
5168.0	-24.9	156.221	5168.0M. TO 6855.0M.	.003	-.184
6855.0	-37.5	161.236	6855.0M. TO 7575.0M.	-.001	.061
7575.0	-40.0	160.624	7575.0M. TO 7779.0M.	-.000	.018
7779.0	-41.3	160.575	7779.0M. TO 26500.0M.	.004	-.540
26500.0	-43.9	230.738			

CLOUD

54

TABLE 2

August 11, 1970, 1200Z, Cloud Density: 50 drops/cm^3

FLUXES AND HEATING RATES

Z,M.	T,C	FLUX	LAYER LIMITS	FLUX DIV.	HEATING
0.0	1.7	-4.927	0.0M. TO 100.0M.	-.005	.175
100.0	2.4	-5.462	100.0M. TO 200.0M.	.001	-.020
200.0	3.1	-5.401	200.0M. TO 299.0M.	.011	-.382
299.0	3.8	-4.276	299.0M. TO 551.0M.	.026	-.502
551.0	2.6	2.348	551.0M. TO 988.0M.	.005	-.104
988.0	.3	4.546	988.0M. TO 1051.0M.	1.352	-27.395
1051.0	1.7	89.717	1051.0M. TO 1875.0M.	.021	-.828
1875.0	-.6	107.377	1875.0M. TO 2587.0M.	.020	-.839
2587.0	-4.5	121.588	2587.0M. TO 4304.0M.	.012	-.592
4304.0	-17.0	143.012	4304.0M. TO 4921.0M.	.013	-.699
4921.0	-23.1	151.058	4921.0M. TO 5044.0M.	.017	-.971
5044.0	-23.8	153.206	5044.0M. TO 5168.0M.	.025	-1.435
5168.0	-24.9	156.362	5168.0M. TO 6855.0M.	.003	-.184
6855.0	-37.5	161.376	6855.0M. TO 7575.0M.	-.001	.061
7575.0	-40.0	160.764	7575.0M. TO 7779.0M.	-.000	.018
7779.0	-41.3	160.715	7779.0M. TO 26500.0M.	.004	-.540
26500.0	-43.9	230.877			

CLOUD ↕ (layers 551.0 – 988.0)

TABLE 3

August 11, 1970, 1200Z, Cloud Density: 80 drops/cm^3

was run for ground albedos from .05 to .85, 10° latitude intervals, and cloud optical depths from .01 (thin haze) to 1 (thin cirrostratus) at both solstices and the equinox. The results indicated that for an optical depth of 1, the absorbed shortwave radiation would be reduced by almost 300 cal/cm^2 day at 20° in the summer hemisphere and by 150 cal/cm^2 day at the summer pole. The latitudinal albedos of Vonder Haar et al. (1971) were used. If the summer pole albedo (without the thin cloud) were reduced from .60 to the global average value of .30, the reduction in absorbed radiation could be as high as 350 cal/cm^2 day. The infrared effect of such a cloud will depend critically on cloud height, but calculations with cirrus at the tropopause and at the −40° C isotherm suggest much less contrast between summer and winter hemispheres in the longwave component. The overall effect of a thin cloud layer would appear to be a reduction in the pole to pole energy budget gradient, at least at solstice. Results for the equinox are more equivocal.

Multiple Layer Model

All of the infrared calculations made thus far have been based on a two-stream approximation with absorption, emission and scattering. Analytic solutions within layers with constant ratios of scattering are matched at the boundaries to give the constants in the equations for the net and total fluxes. The equations for these constants are of the form

$$K_1 = \alpha_1 J_1 + \beta_1$$

$$\left.\begin{array}{l} K_i = A_i J_{i-1} + B_i K_{i-1} + C_i \\ J_i = D_i J_{i-1} + E_i K_{i-1} + F_i \end{array}\right\} \quad i = 2 \text{ through } N$$

$$J_N = \beta_N$$

An algebraic solution was made for $N = 3$, but the number and complexity of the terms made it apparent that direct solutions for larger N's were impractical, while matrix inversion techniques were time-consuming and involved

serious problems with small differences between large terms. The approach being currently worked on involves setting up the equations

$$K_1 = J_1 \gamma(i) + \varepsilon(i)$$

$$J_1 = J_1 \delta(i) + \rho(i),$$

setting up recursion formulas for γ, ε, δ, and ρ, and solving for J_1 by use of the equation for J_N. Partial expansion of the coefficients allows cancellation of many large terms, and the final equations appear as if they should be computationally stable. Final checking of these equations and programming are in process; the completed model will handle up to 5 separate cloud layers with up to 3 different sets of optical parameters.

APPENDIX I

THEORY, INSTRUMENTATION, CALIBRATION AND EXPERIMENTAL PROCEDURE FOR DETERMINING OPTICAL EXTINCTION COEFFICIENTS ARISING FROM ABSORPTION AND SCATTERING FROM ATMOSPHERIC AEROSOLS

G. Shaw

DESCRIPTION OF EXPERIMENTAL METHOD

The direct solar radiation at wavelength λ, $I_o(\lambda)$, decreases in magnitude during its progressive entry into the atmosphere because of scattering and absorption by atmospheric gases and particulates (aerosols). In the visible and near infrared part of the spectrum, absorption by atmospheric gases is primarily due to excitation of vibration rotation bands of tri-atomic molecules such as carbon dioxide, water vapor and ozone. Non-resonant scattering, on the other hand, occurs from all molecules and particulates. Resonant scattering from atoms and molecules and emissive processes such as Raman or fluorescent scattering can be neglected for the experiment reported here.

We make the assumption that the Lambert-Beer law of atmospheric attenuation is valid, and therefore the depletion in intensity arising from absorption and scattering in a height increment dh is expressible as,

$$dI(\lambda,h) = - I(\lambda,h) \sec (z) \, dh \, \beta(\lambda,h) \qquad (1)$$

where $I(\lambda,h)$ = direct solar intensity at wavelength λ and at geometric height h

$z(h)$ = zenith angle of incoming solar ray at height h

$\beta(\lambda,h)$ = volume extinction coefficient (km^{-1}).

Integration of eq. 1 leads directly to an expression for the solar intensity at height h as,

58

$$I(\lambda,h) = I_o(\lambda) \ EXP\left\{-\sec(z)\int_h^\infty \beta(h)dh\right\} \qquad (2)$$

where $I_o(\lambda)$ = solar intensity incident on the top layers of the atmosphere.

The optical depth $\tau(\lambda,h)$ is defined as

$$\tau(\lambda,h) = \int_h^\infty \beta(h)dh \qquad (3)$$

It is assumed that $z \neq z(h)$ which is equivalent to neglecting the curvature of the earth or, said another way, the atmosphere is approximated as being plane parallel; this assumption is valid only provided that the solar elevation angle (90°-z), is larger than about 20°. For lower elevation angles the Bemporad function can be used.

The approximation to the equation of transfer represented by eq. 1 can become invalid for atmospheres containing an emission term (such as fluorescent scattering) or whenever multiple scattering or large optical depths are encountered. For radiation in the visible and near infrared region passing through the earths atmosphere, however, eq. 1 represents a sufficiently good degree of approximation for clear atmospheres (with $\tau(\lambda) << 1$). The requirements, then, for eqs. 1 and 2 to be valid are: (1) the atmospheric optical depth must be small ($\tau < 1$); (2) the solar elevation angle must be greater than about 20°. In addition, equations are invalid for wavelength regions where there is strong absorption by gaseous components or resonant scattering.

The expression provided by eq. 1 forms the basis for the interpretation of the optical airborne equipment that is the subject of this report. Direct solar intensity at several narrow wavelength intervals ($\frac{\Delta\lambda}{\lambda}$ = .02) were monitored with an airborne photometer. Changes in altitude, dh, resulted in small changes in the solar intensity in accordance with the expression given by eq. 1. Thus, by noting the magnitude

of the solar intensity, $I_o(\lambda)$ and the differential change in intensity with height, $dI(\lambda,h)/dh$, it was possible to quantitatively evaluate the optical extinction coefficient, $\beta(\lambda,h)$, by using eq. 1. Furthermore, by employing multiple wavelengths, λ_i, one can then evaluate the extinction coefficient at multiple wavelengths. Knowledge of $\beta(\lambda,h)$ at several diverse wavelengths enables one to deduce some parameters that describe the size spectrum of the atmospheric aerosols contained in the neighborhood of h.

The evaluation of the optical parameter $\beta(\lambda,h)$ is of fundamental interest for modeling the radiative transfer processes in the atmosphere. In particular, our surveillance of the size distribution and height distribution of the atmospheric aerosols has important significance with regard to assessing the "radiation climate" over the pack ice and over the tundra plains of northern Alaska.

THE AIRBORNE PHOTOMETER-INSTRUMENTAL DETAILS

An airborne photometer was constructed for the optical study and is illustrated in Figure 1. The photometer is hand-held and is kept pointed directly at the sun by use of a peep sight. The photometer is carried aloft normally by a Cessna 180 aircraft; the solar disk was viewed by pointing the instrument through a five centimeter hole in the aircraft window.

An interference filter is used to define a narrow wavelength region ($\Delta\lambda/\lambda = 0.02$); provisions are made to change the filter so that several wavelengths can be used. A PIN doped silicon photodetector with an active area of 1 cm^2 is employed in the photometer; it has a usable response extending from about 0.38 microns to 1.15 microns. The incoming light beam is modulated with a mechanical chopper wheel that allows the highly temperature-dependent diode leakage current to be
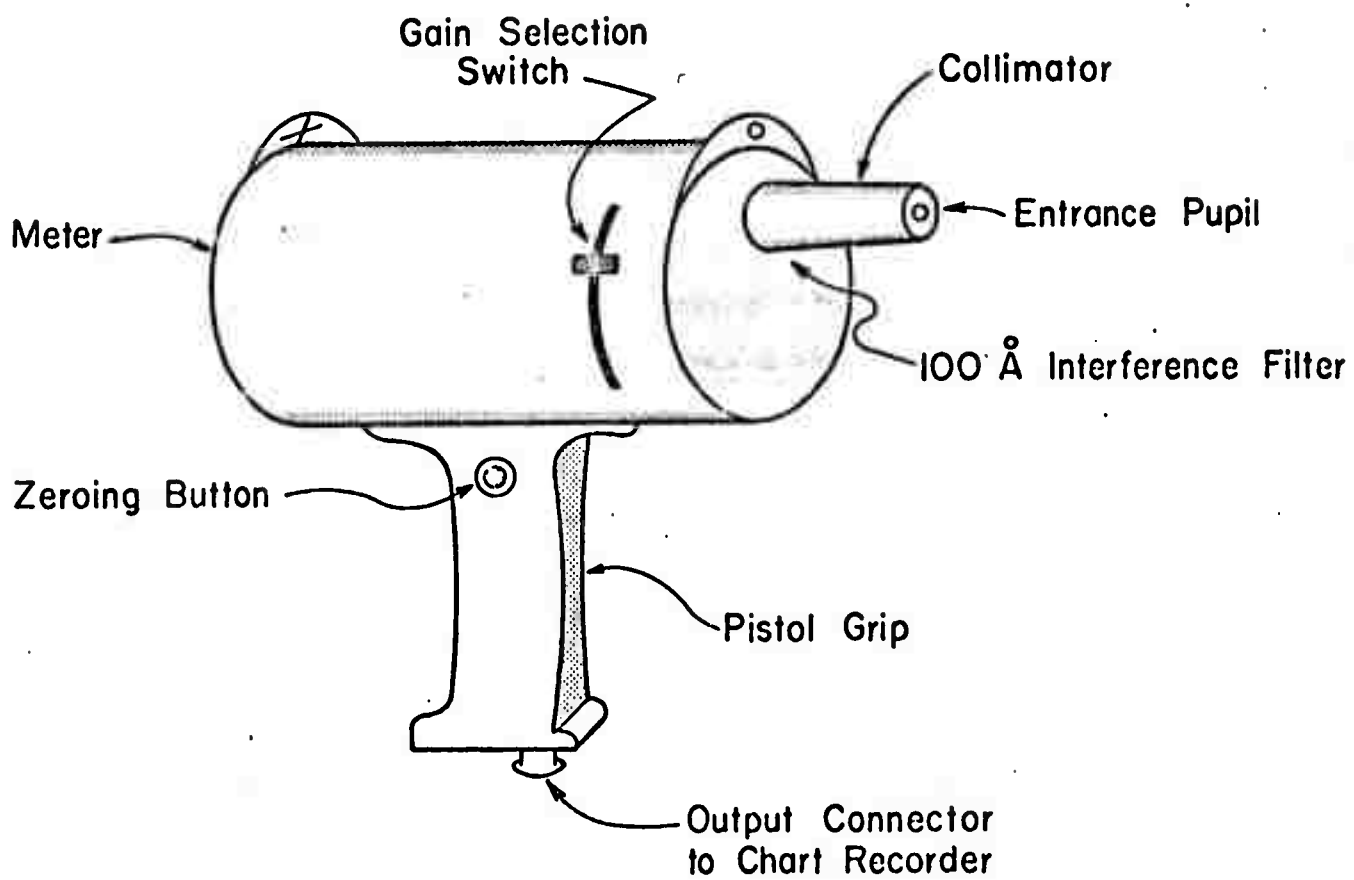
Figure 1.   Illustration of portable airborne sun-photometer.

61

separated from the component of electric current that arises from light impinging upon the photodetector.

The electronic circuitry is designed to amplify the alternating electric current from the photodiode to a level sufficient to operate a portable chart recorder. Operational amplifiers with controlled feedback are used in the electronics to insure constant amplification under a wide range of environmental conditions. The schematic diagram of the photometer electronics is shown in Figure 2.

The solar intensity as observed near the ground undergoes a considerable variation in magnitude as solar elevation angle and/or wavelength are changed, and therefore it is mandatory to incorporate several amplification levels. Four discreet gain levels are available, each differing by a factor of five, and these enable one to obtain a usable signal over a dynamic range of approximately 10^4.

The chart recorder and photometer both operate from a battery pack; the entire system weighs approximately 10 kg and occupies about 0.25 m^3.

FLIGHT DESCRIPTIONS

As mentioned previously, the direct sun photometer was flown aboard an aircraft (Cessna 180). All flights were made near the vicinity of Barrow, Alaska, and started at the Naval Arctic Research Laboratory. A total of eight flights were conducted from the period 4 April 1972 to 18 April 1972. The first half of April was chosen because of favorable chances of clear skies and also because concurrently, surface studies were carried out further north on the pack ice at the AIDJEX camp.

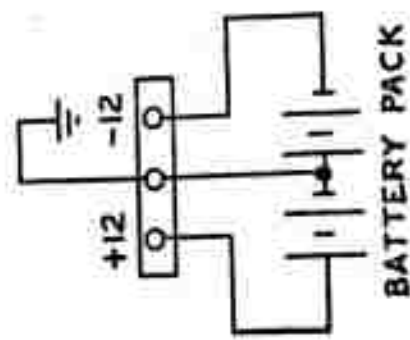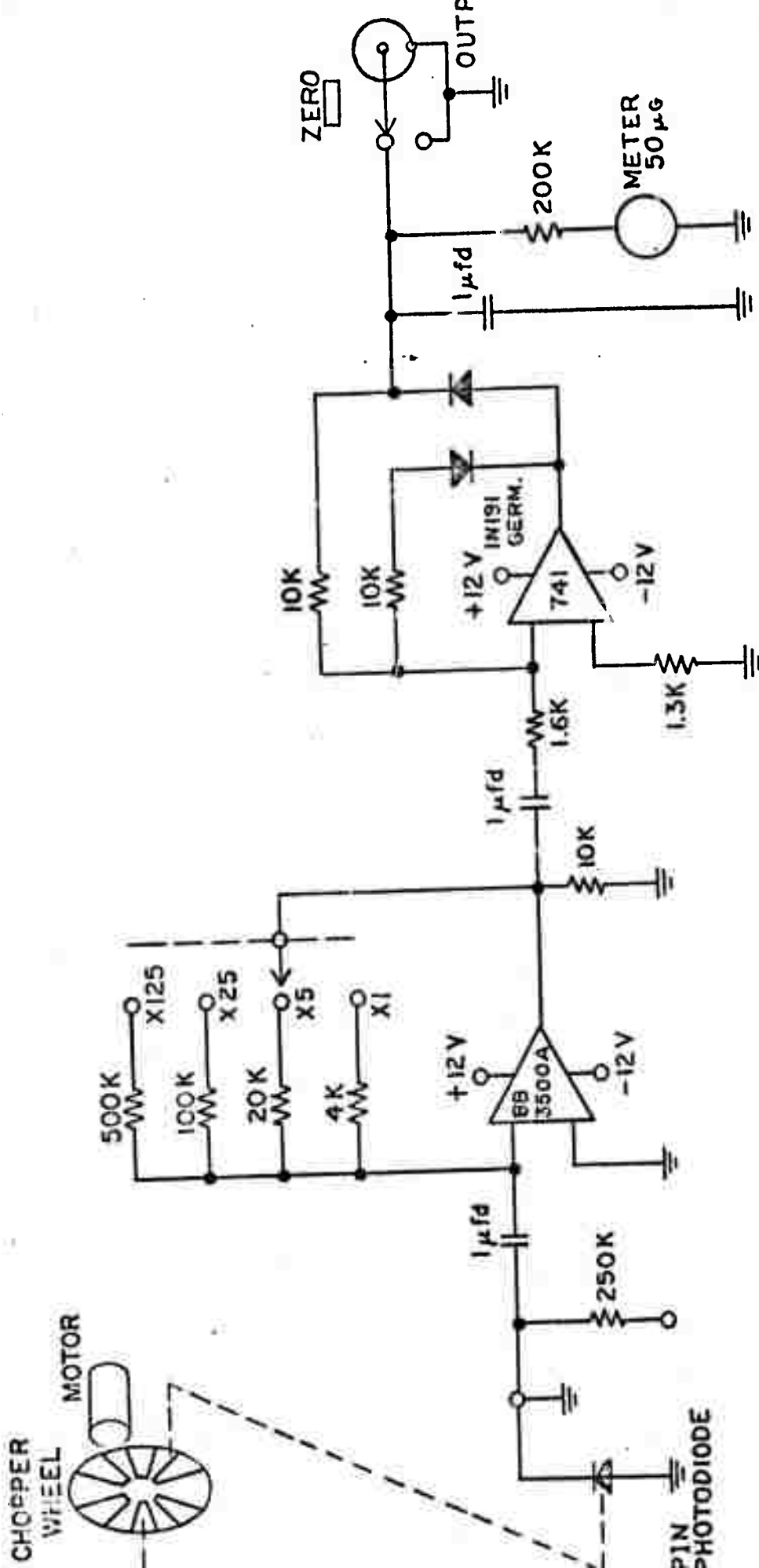Table 1 presents a brief synopsis of all eight flights:

Figure 2. Schematic diagram of electronics used in the sun-photometer.

63

TABLE 1

FLIGHT SCHEDULE - BARROW, ALASKA

Flight No.	Date	Time (GMT)	Max Altitude (1000 ft)
1	4- 6-72	0151-0251	10
2	4- 6-72	2120-2400	10
3	4- 7-72	1930-2014	10
4	4- 8-72	2025-2127	10
5	4-11-72	0038-0153	12
6	4-12-72	0118-0304	15.5
7	4-16-72	2201-2238	10
8	4-18-72	0037-0120	10

A typical flight would involve climbing at a constant rate to some specified altitude ceiling, normally taken as 10,000 feet, all the time keeping the instrument directed toward the sun and recording the output on a chart recorder. As 500 ft increments in altitude were passed, marks were placed on the chart record. Temperature, sky conditions and other relevant information were logged during the flights.

In order to keep the instrument pointed at the sun through the aperture in the aircraft window, it was necessary to fly at a constant azimuth approximately +40° from the sun's vertical. This was because of the geometry imposed by the overhanging aircraft wing and wing strut which would occult the solar disk if the azimuth was not properly adjusted. A typical flight, because of the constraints imposed on bearing and climb-rate, would extend out some 100 miles from the Naval Arctic Research Laboratory at Barrow. Unfortunately, the assumption of horizontal homogeneity over distances of this scale is not necessarily valid, especially during certain synoptic conditions such as when a frontal system is located nearby. To check against the possibility of varying airmasses, we would occasionally maintain a constant altitude for one or two minutes and check to insure that the solar intensity remained constant. Upon occasion, we found, by using this method, that the solar intensity would inexorably decrease (or increase)

64

to indicate that we were entering into a more (or less) turbid air mass.

The occurrence of thin cirrus clouds aloft was of continual concern. In fact, at certain times when the sky was apparently clear, the solar intensity would begin to decrease while flying at a constant altitude until, eventually, one would become aware of very tenuous cirrus ice clouds in the vicinity of the sun. In some instances, the thin cirrus striations or other horizontal homogeneities invalidated the results of a flight. Also, instrumental problems occasionally occurred, notably freezing of the chopper motor, with an attendent noisy signal.

An inspection of the analog records and log book indicates that usable information can be obtained from four flights. The data accumulated on other flights is, for one reason or another, suspect; therefore, these records will not be analyzed.

During a typical flight, the optical filters were placed in the photometer one at a time and data would be accumulated for each color by ascending or descending through the absorbing and scattering layers. Because of the relatively long time involved in reaching a ceiling elevation of 10,000 ft (this would take about a half hour) we limited the number of filters used to two colors centered at 5000 and 7000 Angstroms although a small amount of information was also accumulated at a wavelength of 4000 Angstroms.

DATA REDUCTION

The data consists of analog chart recordings of photometer voltage as a function of altitude, and also miscellaneous notes on meteorological parameters such as sky appearance and temperature. Supplementary information consists of synoptic weather maps at the surface level as well as at 850 mb, 700 mb and 500 mb levels.

Calibration Procedures

In order to interpret the chart recordings one must calibrate the photometer. Calibration of the photometer is necessary for several reasons. Firstly, one must insure that the relationship between the output signal and the incoming light intensity is linear. Secondly, the relation between the output voltage and input intensity in absolute units is desirable because it allows one to assess some additional information about the optical depth of the atmosphere.

The transfer function (ratio of output voltage to input electric current) for the electronic section of the photometer was determined experimentally by replacing the photodiode by an alternating current source. The electronics yielded a linear response over a considerable range of input current. The linearity of the photometer, as well as an estimation for the absolute calibration constant, was further obtained by utilizing a 500 watt quartz halogen lamp as a source of known radiation. A range of input intensities covering several decades was obtained by using calibrated neutral density filters. By this technique it was determined that the photometer is linear to an accuracy of better than two percent over a range of 3 decades of input light intensity.

The output voltage of the photometer that would be developed for zero air mass is of special importance. Knowledge of this constant (for each filter used) enables one to specify immediately the total vertical extinction or optical depth by use of eq. 2.

Successful application of this method depends upon knowledge of the magnitude of the solar intensity, $I_0(\lambda)$, incident upon the atmosphere. Fortunately, the solar intensity in absolute units ($\mu w \ cm^{-2} \ nm^{-1}$) has now been determined to an estimated accuracy of several

percent over the entire visible region (Thekaekara, 1968) and tabulated. Knowledge of the solar topside intensity, $I_o(\lambda)$, and the absolute instrumental constant $k(\lambda)$ then allows one to a-priori specify the optical depth of the atmosphere (viz eq. 2) by

$$\tau(h,\lambda) = \frac{-1}{\sec(z)} \cdot \ln\left(\frac{V(\lambda,h)}{V_o(\lambda)}\right) \tag{4}$$

where $V_o(\lambda) = k(\lambda)I_o(\lambda)$

$\quad$ k $\quad$ = absolute instrumental calibration constant (volts watt^{-1} nm cm^2)

$\quad$ V_o $\quad$ = zero air mass voltage.

As a final point, it is noted that the optical depth of the atmosphere can be determined in an independent fashion by using the Langley method of curve fitting. In order to illustrate this, we note that a plot of log $V(\lambda_o,h)$ against sec(z) would by eq. 4 be linear. Furthermore, the slope of the linear relation is proportional to optical depth, $\tau(\lambda)$, and the intercept of the line onto the ordinate will yield the numerical value for $V_o(\lambda)$ corresponding to topside incident solar radiation $I_o(\lambda)$ can be inferred in an independent fashion from the method utilizing direct calibration from a standard lamp. The two independent methods of determining V_o for λ=5000 Å agreed to within 6%: this is considered to be within the limit of the standard lamp irradiance and might be improved upon in a m exhaustive study.

Inference of Total Extinction Coefficient

The extinction coefficient, $\beta(h,\lambda)$, may be obtained from the data by use of eq. 1. In order to evaluate solar zenith angle at the time of observation, the celestial spherical triangle having vertices at the solar disk, the local zenith, and at the celestial pole, is solved to yield

67

$$\cos(z) = \sin(\ell)\sin(\delta) + \cos(\ell)\cos(\delta)\cos(T_0) \qquad (5)$$

where ℓ = local latitude

  δ = solar declination at time of observation

  T_0 = hour angle referenced to solar noon

The hour angle of the sun, T, is determined by,

$$T_0 = LST-SLD-LLD-E \qquad (6)$$

where LST = local standard time in radians

  SLD = standard longitude difference = 10 hr

  LLD = local longitude at observation place

  E = equation of time

For the wavelength of interest, the extinction coefficient $\beta(h,\lambda)$ is composed of additive terms arising from absorption by atmospheric ozone, $\beta_g(h,\lambda)$, Rayleigh scattering by atmospheric molecules, $\beta_R(h,\lambda)$ and by absorption and scattering from the aerosols, $\beta_D(h,\lambda)$. Written mathematically

$$\beta(h,\lambda) = \beta_g(h,\lambda) + \beta_R(h,\lambda) + \beta_D(h,\lambda) \qquad (7)$$

Rayleigh Scattering

The extinction term arising from Rayleigh scattering is proportional to the number density of molecules and hence to atmospheric pressure. Furthermore, the Rayleigh scattering term has a λ^{-4} dependency and so we can write

$$\beta_R(h,\lambda) = \beta_R(o,\lambda_o) \frac{P(h)}{P(o)} \left(\frac{\lambda_o}{\lambda}\right)^4 \qquad (8)$$

where P(h) = atmospheric pressure at height h.

Taking λ_o=5000 Å $\beta_R(o,\lambda_o)$=1.716x10^{-2} km^{-1} (Elterman, 1968). The variation of pressure with height is taken from the Standard Atmosphere tabulations (Valley, 1965).

Atmospheric Ozone

Atmospheric ozone has broad absorption features in the mid-visible

(the Chappius bands) and hence its influence on our data must be considered. Figure 3a illustrates the molecular absorption cross-section for ozone as a function of wavelength. Figure 3b presents the mean seasonal and latitudinal variation in columnar ozone amount in atmo-cm. The majority of atmospheric ozone is contained in the lower stratosphere (Dutsch, 1971) and the optical depth arising from overburden of ozone is constant for the altitude range of the Cessna 180 flights at Barrow; however, some correction of ozone optical depth with altitude is made for the radiometer data acquired on the later series of Convair 990 flights that extended to 38,000 feet. For these cases, the vertical distribution of ozone was scaled from data presented by Dutsch (1971) for the appropriate season and latitude. It perhaps should be mentioned that the vertical overburden of atmospheric ozone, as can be seen from inspecting Figure 1 (Section V), takes on its largest seasonal value in spring at high latitudes and thus the absorption effects from ozone for our Barrow data obtained in April are quite pronounced.
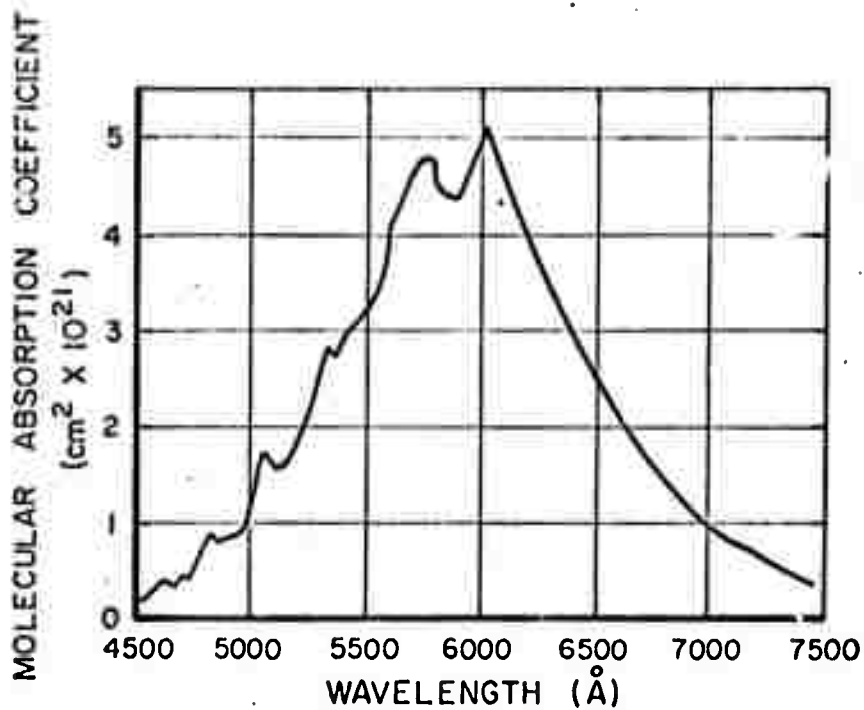
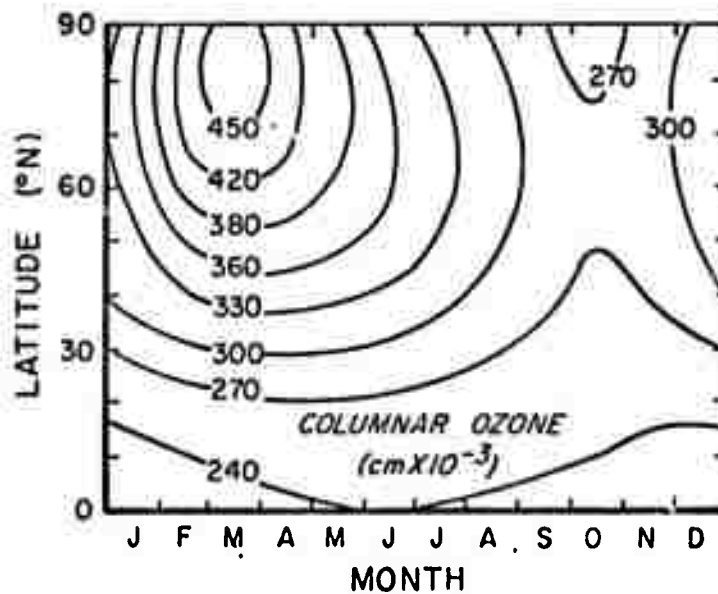Figure 3a. Molecular cross-section of ozone as a function of wavelength.

Figure 3b. Mean seasonal and latitudinal variations in columnar atmospheric ozone amount.

REFERENCES

Albrecht, F., Theoretische Untersuchungen über den Strahlungsumsatz in Wolken, Meteor. Z, 50, 478-486, 1933.

Badgley, F. I., Heat balance at the surface of the Arctic Ocean, Proceedings of the Western Snow Conference, Spokane, Washington, 1961.

Badgley, F. I., Heat budget at the surface of the Arctic Ocean, Proceedings of symposium on Arctic heat budget and atmospheric circulation, RAND RM-5233-NSF, 1966.

Bigg, E. K., Report on ice nucleus workshop, Fort Collins, Aug. 1970, Report of 2nd Int. Workshop on Condensation and Ice Nuclei, 97-105, 1970.

Bowling, Sue Ann, Radiative cooling rates in the presence of ice crystal aerosols, Ph.D. dissertation, University of Alaska, 386 pp., University microfilms, 71-15,060, 1970.

Cronin, J. F., Recent volcanism and the stratosphere, Science, 172, 847, 1971.

Doronin, Y. P., Thermal interaction of the atmosphere and the hydrosphere in the Arctic (Trans. Israel Prog. for Scientific Translation, Leningrad, 1969.

Dutsch, H. V., Advances in Geophysics, 15, 219-322, Academic Press, New York, 1971.

Elsasser, W. E. and M. F. Culbertson, Atmospheric radiation tables, Meteorological Monographs 4, No. 23, 1960.

Elterman, L., UV, visible and IR attenuation for altitudes to 50 km, 1968, Report AFCRL-68-0153, Air Force Cambridge Research Laboratories, 1968.

Fletcher, J. O., The heat budget of the Arctic Basin and its relation to climate, RAND Corp, R-444-PR, 1965.

Fletcher, J. O., Proceedings of the Symposium on the Arctic Head Budget and Atmospheric Circulation, Jan. 31 through Feb. 4, 1966, Lake Arrowhead, California, RAND Corp., Rm 5233 NSF Dec. 1966.

Franceschini, G., The Influence of Clouds on Solar Radiation at Sea, Deutsche Hydrographische Zeitschrift, Heft 4, 162-171, 1968.

Fritz, S., Solar radiant energy and its modification by the earth and its atmosphere, Compendium of Meteorology, Malone (ed) 1951.

Haurwitz, B., Insolation of relation to cloud type, J. of Met., 5, 110-113, 1948.

Hewson, E. W., The reflection, absorption and transmission of solar

radiation by fog and cloud, Quart. Jour. Roy. Meteor. Soc., Vol. LXIX, No. 298, 47-62, 1943.

Irvine, W. M. and J. B. Pollack, Infrared optical properties of water and ice spheres, Icarus, 8, 324-360, 1968.

Loewe, F., On the radiation economy, particularly in the ice- and snow-covered regions, Gerlands Beiträge zur Geophysik, 72 Heft 6, 371-376, 1963.

Maykut, G. A. and N. Untersteiner, Numerical prediction of the thermo-dynamic response of Arctic sea ice to environmental changes, RAND RM-6093-PR, 1969.

Neiburger, M., Reflection, absorption and transmission of insolation by startus cloud, Jour. of Meteor., 6, 98-104, 1948.

Ohtake, T., Cloud settling chamber for ice nuclei count, Proc. Int. Conf. Weather Modification, Sept. 1971, Canberra, 38-41, 1971.

Polar Research, A Survey Committee on Polar Research, National Research Council National Academy of Science, Washington, D. C., pp. 204, 1970.

Shaw, G. and G. Wendler, Atmospheric turbidity measurements at McCall Glacier in northeast Alaska, Presented at Conference on Atmospheric Radiation to be held at Ft. Collins, Colorado, August 7-9, 1972.

Stevenson, C. M., An improved Millipore filter technique for measuring the concentration of freezing nuclei in the atmosphere, Quart. J. Roy. Meteor. Soc., 94, 35-43, 1968.

Thekaekara, M. P.. Solar irradiance measurements from a research aircraft at 38,000 ft., Report X-322-66-304 (Goddard Space Flight Center, Greenbelt, Md.) August 1968.

Vonder Haar, T. H., E. Rascheke, M. Pasternak and W. Bandeen, Measurements of solar energy reflected by the earth and atmosphere from meteoro-logical satellites, Proc. of 1971 Internatl. Solar Energy Soc. Conf. Greenbelt, Maryland, 1971.

Vowinckel, E. and S. Orvig, Relation between solar radiation income and cloud type in the arctic, Arctic Meteorology Research Group, Pub-lication in Meteorology, No. 48, Scientific Report No. 3, Contract No. AF 19(604)-7415, Project No. 8623-Task No. 86230, pp. 26, 1962.

Vowinckel, E. and S. Orvig, Insolation and absorbed solar radiation at the ground in the arctic, Arctic Meteorology Research Group, Pub-lication in Meteorology No. 53, Scientific Report No. 5, Contract No. AF 19(604)-7415, Project No. 8623-Task No. 862303, pp. 32, 1962.

Weller, G. and P. Schwerdtfeger, Radiation penetration in antarctic plateau and sea ice, WMO Technical Note No. 87, 12C, 1967.

Weller, G., Radiation diffusion in antarctic ice media, Nature, 221(5178), 355, 1969.

Zdunkowski, W. G., R. E. Barth and F. A. Lombardo, Discussion on the atmospheric radiation tables by Elsasser and Culbertson, Pure Appl. Geophys., 63, 211-219, 1966.